



# Role of atmospheric heat fluxes and ocean advection on decadal (2000–2019) change of sea-ice in the Arctic

A. Mukherjee<sup>1</sup> · M. Ravichandran<sup>2</sup>

Received: 17 September 2021 / Accepted: 1 October 2022 / Published online: 11 October 2022  
© The Author(s), under exclusive licence to Springer-Verlag GmbH Germany, part of Springer Nature 2022

## Abstract

In this article, role of ocean advection and atmospheric heat fluxes on recent decadal (2000–2019) decrease of sea-ice in the Arctic (60° N–90° N) has been investigated using an ocean sea-ice coupled model, known as Modular Ocean Model of version 5 with Sea Ice Simulator (MOM5SIS). MOM5SIS successfully simulates AVHRR observed decadal change of sea-ice concentration (SIC) and sea surface temperature (SST) in the Arctic during all four seasons; winter (December–February), spring (March–May), summer (June–August) and autumn (September–November) except few occasions. Also, best performance of the MOM5SIS are restricted at south of 80° N with statistical significance of more than 90%. We have also divided Arctic Ocean into eight sectors for our detailed analysis. Maximum decadal decrease of SIC and increase of SST has been observed in the Barents (sector 2), Kara (sector 3) and Laptev (sector 4) Sea regions of the Arctic using both AVHRR and MOM5SIS with statistical significance of 90%. Also, very small decadal decrease (increase) of SIC (SST) has been observed in the Norwegian (sector 1) and Beaufort (sector 7) Sea regions of the Arctic using both AVHRR and MOM5SIS. Mixed layer heat budget has been performed to understand role of thermodynamics processes on decadal change of SIC and SST in the Arctic. Strong decadal change of net atmospheric heat (NAH) fluxes are responsible for high decadal change of SIC and SST in the Barents (sector 2), Kara (sector 3) and Laptev (sector 4) Sea regions of the Arctic. In the Norwegian (sector 1) and Beaufort (sector 7) Sea, strong destructive interference between decadal change of NAH fluxes and ocean advection play an important role for small decadal change of SIC and SST during all four seasons. Also, for ocean advection, horizontal part dominate compared to vertical in all eight sector of the Arctic.

**Keywords** Global sea-ice model · Arctic Ocean · Recent decadal change · Sea-ice concentration · Sea surface temperature · Ocean heat budget analysis · Net atmospheric heat fluxes · Ocean advection

## 1 Introduction

It is well known that Arctic sea-ice extent is declining rapidly compared to Antarctic and play a major role for global climate variability (Bore and Yu 2003; Comiso et al. 2017; Wunderling et al. 2020; Previdi et al. 2021; Kim et al. 2022). Maximum decline of sea-ice extent, which has been quantified as sea ice concentration (SIC), are observed in the Barents, Kara and Laptev Sea regions of the Arctic during summer and autumn seasons (Drobot et al. 2006; Holland

et al. 2006; Serreze et al. 2007; Perovich et al. 2011; Holland et al. 2011, 2019). Satellite observation shows rapid decline of Arctic SIC from 1978 (Hansen et al. 2010; Stroeve and Notz 2018; Gascard et al. 2019). Rapid melting of Arctic sea-ice during summer seasons and associated increase of sea surface temperature (SST) are responsible for global weather and climate change, sea-level rise etc. (Stroeve et al. 2007; Budikova 2009; Stroeve et al. 2012; Box et al. 2019). So, process studies related to decadal reduction of Arctic SIC is a global interest of research at present.

Various model studies using reanalysis products and coupled sea-ice model showed possible dynamics and thermodynamics processes associated with rapid decline of sea-ice in the Arctic (Steele et al. 2010; Stroeve et al. 2012; Massonnet et al. 2018; Zou et al. 2021). It has been observed that decadal change of net longwave and shortwave radiation in the lower atmosphere has a strong impact on

✉ A. Mukherjee  
amukherjee.physics@gmail.com

<sup>1</sup> ESSO-National Centre for Polar and Ocean Research (NCPOR), Ministry of Earth Sciences (MoES), Vasco da Gama, Goa, India

<sup>2</sup> Ministry of Earth Sciences (MoES), New Delhi, India

interannual and decadal variability of SST and SIC in the Arctic (Jungclauss and Koenigk 2010; Ohmura 2012; Holland and Landrum 2015; Kapsch et al. 2016). Recent decadal increase of downward shortwave radiation in the Arctic associated with greenhouse gases and aerosole particles has a strong impact on decadal increase of SST and decrease of SIC in above regions (Wang and Key 2003, 2005; Holland and Landrum 2015; Juszak et al. 2017). Similarly, recent increase of downward longwave radiation associated with increase air temperature, cloudiness, green house gases like water vapour, CO<sub>2</sub> etc. and aerosole particles are responsible for Arctic warming and sea-ice loss (Wang and Key 2003, 2005; Ohmura 2012; Linden et al. 2017). In the recent decade, air temperature in the Arctic has increased significantly of the order of  $\sim 2^{\circ}\text{C}$  and altered air-sea interactions (Overland et al. 2019; Przybylak and Wyszynski 2020). Decadal increase of atmospheric downward radiation flux also responsible for change of atmospheric circulation in the lower atmosphere and associated change of latent and sensible heat fluxes (Praetorius et al. 2018; Zhang et al. 2021; Li et al. 2022). Overall, based on previous research, it has been concluded that decadal change of net atmospheric heat flux play a major role for decadal variability of SST and SIC in the Arctic (Jungclauss and Koenigk 2010; Ohmura 2012; Holland and Landrum 2015; Kapsch et al. 2016; Cao et al. 2018; Ming et al. 2021).

Apart from atmospheric net heat fluxes, ocean advection also play a significant role on decadal warming of Arctic (Zhang and Li 2017; Asbjornsen et al. 2019; Linden et al. 2019; Timmermans and Marshall 2020; Polyakov et al. 2020; Ricker et al. 2021). Advection of ocean water play a critical role by bringing warmer Atlantic and Pacific water to Arctic Ocean and responsible for increasing SST and melting of sea-ice in the Arctic (Kim and Kim 2019; Linden et al. 2019; Polyakov et al. 2020). Model studies also showed impact of oceanic vertical processes on recent decadal change of Arctic SIC and SST by transporting warmer Atlantic and Pacific water to the Arctic (Ramudu et al. 2018; Liang and Losch 2018; Kim and Kim 2019). Ocean advection processes also significantly strengthened by formation of Beaufort gyre and mesoscale eddies in the Arctic and responsible for decadal variability of Arctic SST and SIC (Proshutinsky et al. 2002; Chatterjee et al. 2018; Amritage et al. 2020). Another critical factor for decadal variability of SIC and SST in the Arctic comes from ocean internal variability (England et al. 2019; Bonan et al. 2021). Previous model studies showed various mechanisms related to formation of ocean internal variability, like Atlantic Meridional Overturning Circulation (AMOC), ocean internal instability etc. (Cheng et al. 2016; Timmermans and Marshall 2018; Liu et al. 2019) play a major role for decadal change of SIC and SST in the Arctic.

Based on various previous model studies, it is well known that net atmospheric heat fluxes (Jungclauss and Koenigk 2010; Ohmura 2012; Holland and Landrum 2015; Kapsch et al. 2016) and ocean advection (Carmack et al. 2015; Aksenov et al. 2016; Oldenburg et al. 2018; Kim and Kim 2019; Ricker et al. 2021; Tsubouchi et al. 2021) play a major role in Arctic warming. Recent study in the Arctic shows a rapid decreasing trend of Arctic summer sea-ice from 2000 (Swart et al. 2015) with record minimum sea-ice extend during 2012 (Parkinson and Comiso 2013), which highlights importance of the study related to recent decadal change (decade between 2010–2019 and 2000–2009) of Arctic SIC and SST using both satellite observations and model. Also, no systematic study has been performed regarding significance of net atmospheric heat flux and ocean advection on recent decadal (2000–2019) change of Arctic sea-ice and SST using heat-budget analysis.

In this study, the contribution of oceanic advection and net atmospheric heat fluxes on recent decadal change of SST and SIC using heat budget analysis has been derived using a global ocean sea-ice coupled model for the eight sectors of the Arctic, which includes Norwegian, Barents, Kara, Laptev, East Siberian, Chukchi, Beaufort and Greenland Sea. The manuscript has been organized as follows. Section 2 describes observed data and model details. AVHRR observed and model simulated decadal climatology of SIC and SST in the Arctic during all four seasons (winter, spring, summer and autumn) has been discussed in the Sect. 3. Observed and mode simulated decadal change (between decade of 2010–2019 and 2000–2009) of SIC and SST in the Arctic has been discussed in Sect. 4. Section 5 discussed thermodynamics processes associated with decadal change of SST and SIC in the Arctic using upper ocean heat budget analysis during four seasons (winter, spring, summer and autumn). Section 6 concludes the paper.

## 2 Data and model

In this section, details of observed data and ocean sea-ice coupled model has been discussed.

### 2.1 Observed data

Satellite derived Advanced Very High Resolution Radiometer (AVHRR) data of SIC and SST has been used for detailed validation of MOMSIS model. AVHRR data is available with  $25\text{ km} \times 25\text{ km}$  of horizontal resolution and daily temporal resolution. Detailed documentation of AVHRR can be downloaded from <https://daac.ornl.gov/FIFE/Datasets/>

[Satellite\\_Observations/Satellite\\_AVHRR\\_Extracted\\_Data.html#url](#).

## 2.2 Global ocean sea-ice coupled model

A global ocean sea-ice coupled model based on coupling between Modular Ocean Model (MOM) of version 5 and ice model known as Sea ice simulator (SIS) has been used for detailed study here. The horizontal resolution of the model (defined as MOMSIS) are set to  $0.25^\circ \times 0.25^\circ$  globally. There are total 50 vertical level in the model with 10 m resolution from surface to 220 m. Tripolar grid has been used in the model with poles over Eurasia, North America and Antarctica to avoid polar filtering over Arctic (Murray 1996). Horizontal and vertical advection of momentum and tracer fields (temperature and salinity) in the MOMSIS are based on multi dimensional piece-wise parabolic method (MDPPM) of Dunne et al. (2012). Smagorinsky Laplacian and Biharmonic schemes described in Griffies and Hallberg (2000) has been used for horizontal mixing of momentum and tracers. Similarly, K-profile parameterization (KPP) schemes has been used for vertical mixing of momentum and tracers in the MOMSIS (Large et al. 1994). Sea surface salinity is relaxed to monthly global climatology of Chatterjee et al. (2012) with 60 days time scale in order to include the impact of river runoff forcing in the MOMSIS implicitly.

SIS component of MOMSIS is a three vertical layer model with one snow and two ice layers. There are total five categories of ice thickness in the SIS. Estimation of Internal stresses of ice in the SIS are based on elastic-viscous-plastic techniques of Hunke and Dukowicz (1997). The thermodynamics of ice is estimated using Semtner three-layer scheme of Winton (2000). Detailed documentation of MOMSIS are available in Delworth et al. (2006).

MOMSIS starts with global temperature and salinity climatology of Chatterjee et al. (2012) during month of January. The model is forced with CORE-II atmospheric forcing (Large and Yeager 2008) of air pressure at 2 m, downward and longwave radiation at 2 m, air temperature at 2 m, specific humidity at 2 m, precipitation at 2 m, snowfall at 2 m and wind stress at 10 m with horizontal resolution of  $2^\circ \times 2^\circ$ . After 100 year of climatological spin-up, MOMSIS starts with real-time atmospheric forcing from January 1979 using ECMWF ERA5 (Wang et al. 2019) with horizontal resolution of  $0.25^\circ \times 0.25^\circ$  and temporal resolution of 6 h. In this manuscript, model outputs between January 2000 to December 2019 has been analysed for decadal change of SIC and SST in the Arctic Ocean defined between  $0^\circ$  E– $360^\circ$  E,  $60^\circ$  N– $90^\circ$  N.

## 2.3 Validation

In this manuscript, entire Arctic regions has been divided into eight sectors; five in the east and three in the west. Eight major sector named as S01, S02, S03, S04, S05, S06, S07 and S08 includes major part of Norwegian, Barents, Kara, Laptev, East Siberian, Chukchi, Beaufort and Greenland Sea respectively. Detailed of above Arctic sector regions are described in Table 1 and also showed in Fig. 1.

Very high correlation (R) with maximum value of more than 0.8 has been observed for SIC between AVHRR and MOMSIS in the Barents (part of S02), Kara (part of S03), Laptev (part of S04), East Siberian (part of S05), Chukchi (part of S06) and Beaufort Sea (part of S07) regions of the Arctic compared to Norwegian (part of S01) and Greenland (part of S08) Sea regions (Fig. 1). However, the performance of the MOMSIS are slightly better in simulation of AVHRR observed SST compared to SIC in almost every sectors of the Arctic. Higher R values has been observed for SST in the Norwegian (part of S01) and Greenland (part of S08) Sea regions of the Arctic compared to SIC (Fig. 1). It is important to note that SST in the model has been estimated using water temperature below sea-ice. Also, a root mean percentage error (RMPE) for SIC and SST has been estimated with low RMPE (less than 40%) at almost every sectors of the Arctic except few locations (Fig. 1). RMPE defines average absolute percentage error for a fixed time period (here 20 years) divided by AVHRR values. Detailed long-term climatological validation of SIC and SST between AVHRR and MOMSIS are discussed in the supplementary material (Figures S1–S4). Validation of MOMSIS in simulation of AVHRR observed decadal climatology and change of both SIC and SST has been discussed in Sects. 3 and 4.

**Table 1** Detailed list of latitude and longitude ranges, which has been used for different sector regions in the Arctic

Location	Longitude average ° E	Latitude average ° N
Sector 01 (S01)	$0^\circ$ E– $30^\circ$ E	$60^\circ$ N– $90^\circ$ N
Sector 02 (S02)	$30^\circ$ E– $60^\circ$ E	$60^\circ$ N– $90^\circ$ N
Sector 03 (S03)	$60^\circ$ E– $90^\circ$ E	$60^\circ$ N– $90^\circ$ N
Sector 04 (S04)	$90^\circ$ E– $150^\circ$ E	$60^\circ$ N– $90^\circ$ N
Sector 05 (S05)	$150^\circ$ E– $180^\circ$ E	$60^\circ$ N– $90^\circ$ N
Sector 06 (S06)	$180^\circ$ E– $210^\circ$ E	$60^\circ$ N– $90^\circ$ N
Sector 07 (S07)	$210^\circ$ E– $270^\circ$ E	$60^\circ$ N– $90^\circ$ N
Sector 08 (S08)	$270^\circ$ E– $360^\circ$ E	$60^\circ$ N– $90^\circ$ N

Sector has been designed based on regions of eight major seas in the Arctic. Here, S01, S02, S03, S04, S05, S06, S07 and S08 represents major part of Norwegian, Barents, Kara, Laptev, East Siberian, Chukchi, Beaufort, Greenland Sea respectively. Eight major Seas of the Arctic also shown in Fig. 1

### 2.4 Statistical significance

In order to estimate 90% statistical significance correlation for SIC and SST between AVHRR and MOMSIS, method discussed in the appendix of Shankar (1998) has been used. Total 20 year of data between 01 January 2000 to 31 December 2019 with 3655 degree of freedom has been used for estimation of correlation and statistical significance. For low-pass filtered data, similar filter has been applied for random number series as discussed in Shankar (1998). For 90% statistical significance level, correlation value of 0.1 (0.6) is fixed for unfiltered (~ 400 days low-pass filtered) data with degree of freedom of 3655.

Statistical student t-test has been performed for decadal change analysis of SIC, SST and SST rate using AVHRR and MOMSIS. Similar student t-test analysis also performed for mixed layer heat budget analysis as discussed in Sect. 5. For above statistical analysis, 365 days daily climatological data for 2 decade (01-January-2000 to 31-December-2009 and 01-January-2010 to 31-December-2019) with 400 days low-pass filter has been used. The formula used for student t-test analysis is given below:

$$t_{value} = \frac{abs(\bar{X}_1 - \bar{X}_2)}{\sqrt{(\frac{S_1^2}{N_1} + \frac{S_2^2}{N_2})}} \tag{1}$$

In Eq. 1,  $t_{value}$ ,  $\bar{X}_1$  and  $\bar{X}_2$  represents t-value, mean of first group, mean of second group respectively.  $S_1, S_2, N_1, N_2$  represents standard deviation of group 1, standard deviation of group 2, number of observations in group 1 and number of observations in group 2 respectively. T-critical value for 90% statistical significance (1.646) with total degree of freedom of 728 (365 + 365 - 2) is obtained from table chart freely

available on <https://www.scribbr.com/statistics/students-t-table/>. T-value higher than t-critical of 1.646 is considered 90% statistical significance. Student statistical significance analysis for decadal change are described in Table 2.

### 3 Observed and model simulated decadal climatology of SIC and SST in the Arctic

In this section, detailed decadal climatological validation of the MOMSIS in simulation of AVHRR observed SIC and SST in the Arctic (60° N–90° N) has been discussed. Here, decadal climatology of SIC and SST has been computed by removing annual variability using 400 days low pass 4<sup>th</sup> order Butterworth time series filter. Decadal climatology of the Arctic has been analysed for four seasons; winter (December–February), spring (March–May), summer (June–August) and autumn (September–November).

High values of R and low values of RMPE has been observed for filtered SIC and SST between AVHRR and MOMSIS (Fig. 2). Due to low-pass filter, statistical 90% significance value for R has increased from 0.1 to 0.6. In the high latitude Arctic regions (80° N–90° N), small R value has been observed which are less than 90% statistical significance. In other parts of the Arctic (60°–80° N), higher R value of more than 0.6 with 90% statistical significance has been observed for above filtered SIC and SST between AVHRR and MOMSIS.

Very good comparison has been observed for decadal climatological SIC between AVHRR and MOMSIS during both winter and spring seasons in all eight sectors of the Arctic, but with slight smaller magnitude (Fig. 3). As an example, in the Barents (part of S02) Sea regions of the Arctic, AVHRR shows average strength of SIC with 50.8% and 52.27% during winter and spring seasons respectively (Table 3). MOMSIS model also shows slight smaller strength of SIC with 37.8% and 42.1%

**Table 2** Statistical student t-test result for decadal change (between decade of 2010–2019 and 2000–2009) of SIC, SST and SST rate using AVHRR and MOMSIS along with MLD heat budget terms related to MLT rate, NAH flux, Ocean advection and residual processes

Location	S01	S02	S03	S04	S05	S06	S07	S08
	t-value	t-value	t-value	t-value	t-value	t-value	t-value	t-value
AVHRR (SIC)	<b>22.39</b>	<b>2.64</b>	<b>9.08</b>	<b>4.97</b>	<b>1.81</b>	1.27	0.41	<b>6.24</b>
AVHRR (SST)	<b>5.99</b>	<b>11.09</b>	<b>10.24</b>	<b>6.93</b>	<b>2.56</b>	1.34	0.15	<b>2.18</b>
AVHRR (SST rate)	0.10	0.10	0.09	0.09	0.08	0.04	0.08	0.03
MOMSIS (SIC)	<b>6.56</b>	<b>8.50</b>	<b>5.27</b>	<b>6.18</b>	<b>4.31</b>	<b>5.10</b>	<b>4.95</b>	<b>3.21</b>
MOMSIS (SST)	<b>5.05</b>	<b>8.64</b>	<b>7.43</b>	<b>10.80</b>	<b>4.98</b>	<b>5.29</b>	<b>7.60</b>	<b>2.11</b>
MOMSIS (SST rate)	0.03	0.03	0.01	0.04	0.02	0.02	0.05	0.03
MOMSIS (MLT rate)	0.18	0.11	0.0001	0.08	0.13	0.04	0.002	0.05
MOMSIS (NAH flux)	0.72	1.05	<b>2.30</b>	<b>2.88</b>	<b>1.89</b>	0.93	<b>3.30</b>	0.56
MOMSIS (advection)	<b>11.14</b>	<b>2.77</b>	<b>7.25</b>	<b>22.65</b>	<b>8.23</b>	0.83	<b>14.31</b>	0.41
MOMSIS (residual)	0.39	<b>1.78</b>	<b>2.32</b>	<b>4.56</b>	<b>2.01</b>	0.69	1.26	0.77

Detailed procedure of T-test analysis are described in Sect. 2.4. T-value higher than t-critical of 1.646 (90% significant with total degree of freedom of 728 (365 + 365 - 2)) has been highlighted in bold font

**Table 3** List of data estimated for average value of decadal climatology of SIC (%) and SST (°C) based on Figs. 3, 4, 5, and 6

Location	SIC	SIC	SIC	SIC	SST	SST	SST	SST
	Winter	Spring	Summer	Autumn	Winter	Spring	Summer	Autumn
	(%)	(%)	(%)	(%)	(°C)	(°C)	(°C)	(°C)
S01 (AVHRR)	55.95	58.22	54.78	52.77	4.70	4.56	5.54	5.59
S02 (AVHRR)	50.84	52.27	46.58	44.60	1.48	1.28	2.49	2.57
S03 (AVHRR)	74.14	77.42	64.18	61.69	− 0.69	− 0.86	0.13	0.20
S04 (AVHRR)	86.20	87.79	76.59	75.56	− 1.22	− 1.34	− 0.74	− 0.69
S05 (AVHRR)	82.34	84.46	74.42	72.75	− 0.87	− 0.99	− 0.30	− 0.25
S06 (AVHRR)	74.86	77.80	65.97	63.67	− 0.29	− 0.45	0.65	0.73
S07 (AVHRR)	89.12	90.10	82.16	81.62	− 1.24	− 1.32	− 0.80	− 0.80
S08 (AVHRR)	63.07	65.79	56.37	54.38	2.38	2.29	3.20	3.23

For estimating decadal climatology, annual variability from SIC and SST has been removed using 400 days low-pass 4<sup>th</sup> order Butterworth time series filter. Decadal climatology has been computed for decade between 01 January 2010 to 31 December 2019

during above two seasons respectively. During summer and autumn seasons, MOMSIS shows good comparison in simulation of AVHRR observed decadal climatological SIC, but with lower magnitude as observed during other seasons (Fig. 4). MOMSIS also successfully simulates AVHRR observed maximum decadal strength of SIC in the western Arctic which includes Greenland (part of S08), Beaufort (part of S07) and Chukchi (part of S06) Sea regions, but with slightly smaller strength. As an example in the Beaufort Sea (part of S02), AVHRR observed decadal climatological SIC has a magnitude of 82.1% and 81.6% during summer and autumn seasons respectively (Table 3). Model MOMSIS also shows decadal climatological strength of SIC with 60.7% and 60.1% during above two seasons respectively.

Very good comparison has been observed using MOMSIS in simulation of AVHRR observed decadal climatological SST in the entire Arctic during winter and spring seasons (Fig. 5). As observed during winter seasons, model MOMSIS successfully simulates AVHRR observed higher positive SST in the Barents (part of S02), Norwegian (part of S01) and Greenland (part of S08) Sea regions of the Arctic during winter and spring seasons. As an example, in the Norwegian (part of S01) Sea regions, AVHRR shows average SST of 4.70 °C and 4.56 °C during winter and spring seasons respectively (Table 3). MOMSIS also shows almost similar strength of SST with magnitude of 4.34 °C and 4.26 °C during above two seasons respectively. Similar very good comparison has been observed using MOMSIS in simulation of AVHRR observed decadal climatological SST during summer and autumn

seasons in the entire Arctic, but with slight higher values (Fig. 6). Also, it has been observed that the performance of MOMSIS is slightly better in simulation of decadal climatological SST compared to SIC during summer and autumn seasons (Figs. 4 and 6).

#### 4 Observed and model simulated decadal change of SIC and SST in the Arctic

In this section, decadal change (decade of 2010–2019 and 2000–2009) of SIC and SST has been compared between model MOMSIS and AVHRR observations. Annual variability from SST and SIC has been removed using 400 days Butterworth low-pass 4<sup>th</sup> order time series filter in order to estimate decadal change. Analysis of student t-test for decadal change showed 90% statistical significance at Norwegian (part of S01), Barents (part of S02), Kara (part of S03), Laptev (part of S04), East Siberian (part of S05) and Greenland (part of S08) Sea regions for both SIC and SST using AVHRR (Table 2). However, MOMSIS shows 90% statistical significance at all eight sectors of the Arctic.

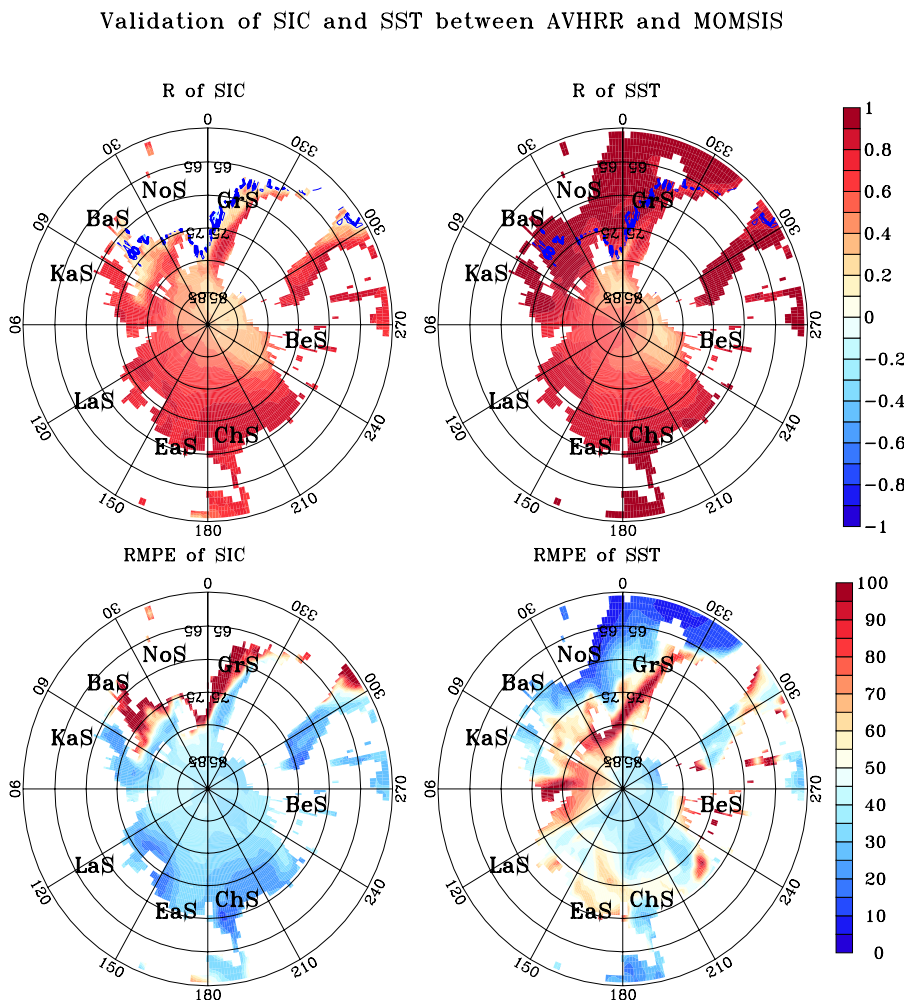
It has been observed that R values for SIC and SST between AVHRR and MOMSIS are below 90% statistical significance in the north of 80° N. So, AVHRR observed small decadal increase of SIC and decrease of SST are not well simulated by MOMSIS at north of 80° N in the Arctic during all four seasons (Figs. 7, 8, 9 and 10).

**Table 4** List of data estimated for average value of decadal change of SIC (%) and SST (°C) based on Figs. 7, 8, 9 and 10

Location	SIC Winter (%)	SIC Spring (%)	SIC Summer (%)	SIC Autumn (%)	SST Winter (°C)	SST Spring (°C)	SST Summer (°C)	SST Autumn (°C)
S01 (AVHRR)	-0.49	0.13	0.05	-0.97	0.31	0.11	0.12	0.24
S02 (AVHRR)	-2.67	-1.98	-2.27	-3.23	0.54	0.41	0.56	0.61
S03 (AVHRR)	-4.35	-3.08	-4.97	-6.24	0.37	0.18	0.49	0.59
S04 (AVHRR)	-1.15	-0.36	-3.69	-4.56	0.17	0.00	0.25	0.36
S05 (AVHRR)	0.53	1.71	0.26	-1.12	0.06	-0.11	-0.03	0.08
S06 (AVHRR)	-1.06	0.06	-0.95	-2.11	0.17	-0.02	0.10	0.24
S07 (AVHRR)	-0.21	0.23	-1.67	-2.41	0.09	-0.06	0.07	0.17
S08 (AVHRR)	2.01	2.74	2.31	1.44	0.12	0.05	0.09	0.14

In order to estimate decadal change, annual variability from SIC and SST has been removed using ~ 400 days low-pass 4<sup>th</sup> order Butterworth time series filter. Decadal change has been estimated by subtracting decadal climatology between decade of 2010–2019 and 2000–2009

**Fig. 1** Left panel of the figure shows correlation (R, top) and root mean percentage error (RMPE, bottom) between AVHRR observed Sea ice concentration (SIC) and model MOMSIS. Right panel of the figure shows R (top) and RMPE (bottom) for Sea surface temperature (SST). Time series daily data between 01 January 2000 to 31 December 2019 has been used for estimation of R and RMPE values in the Arctic regions. R values within blue contour (between -0.1 to 0.1) imply statistical significance of less than 90%. Eight major sea written in the bold font imply dominance of above sea for that regions. Detailed regions of the sector related to eight Arctic major Seas has been described in Table 1. In the figure, NoS, BaS, KaS, LaS, EaS, ChS, BeS and GrS represents Norwegian Sea, Barents Sea, Kara Sea, Laptev Sea, East Siberian Sea, Chukchi Sea, Beaufort Sea and Greenland Sea respectively

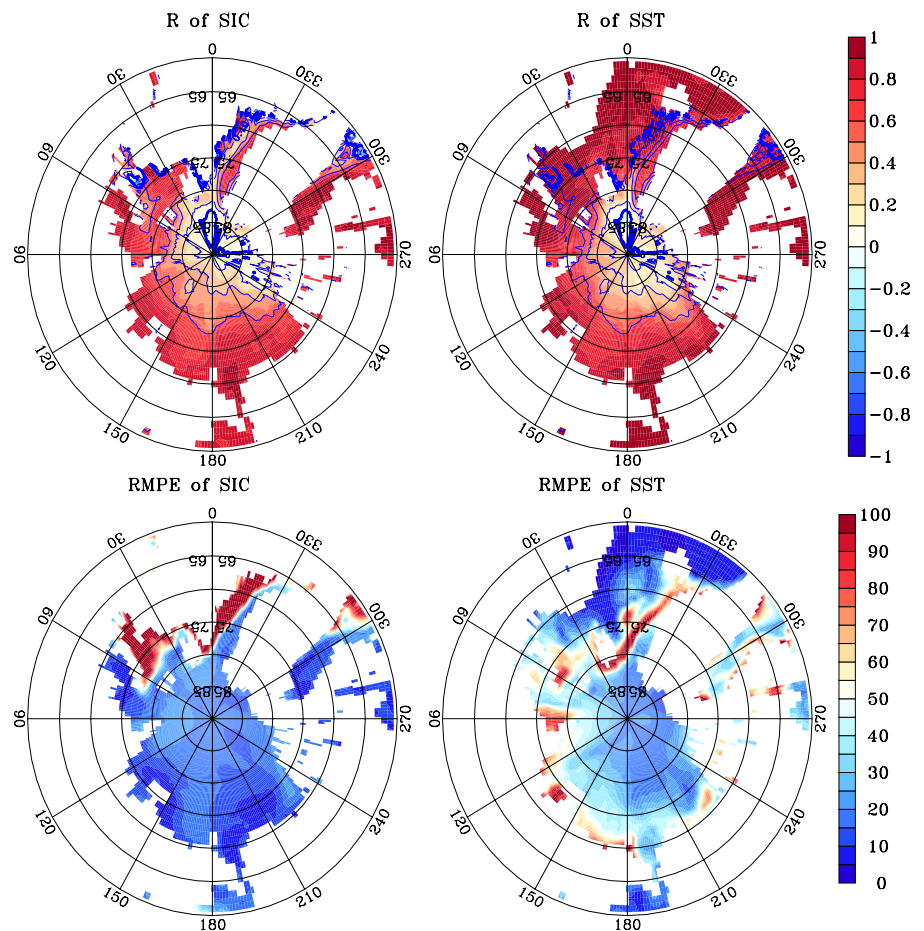


AVHRR shows maximum decadal reduction of SIC in the Barents (part of S01), Kara (part of S02) and Laptev (part of S03) Sea regions of the Arctic during winter and

spring seasons (Fig. 7). MOMSIS also successfully simulates maximum decadal reduction of SIC in above regions during above seasons. As an example, in the Barents

**Fig. 2** Left panel of the figure shows correlation (R, top) and root mean percentage error (RMPE, bottom) between ~ 400 days low-pass (LP) filtered AVHRR observed SIC and model MOMSIS. Right panel of the figure shows similar R (top) and RMPE (bottom) for ~ 400 days low-pass filtered SST. Daily time series data between 01 January 2000 to 31 December 2019 has been used for estimation of R and RMPE values in the Arctic regions. R values within blue contour (between -0.6 to 0.6) are less than 90% statistical significance

Validation of 400 day LP filtered SIC and SST between AVHRR and MOMSIS



(part of S02) Sea regions, AVHRR shows average decadal change of SIC with -2.7% and -2.0% during winter and spring seasons respectively (Table 4). MOMSIS also shows similar average decadal change of SIC with higher values of -7.1% and -6.1% during above seasons respectively.

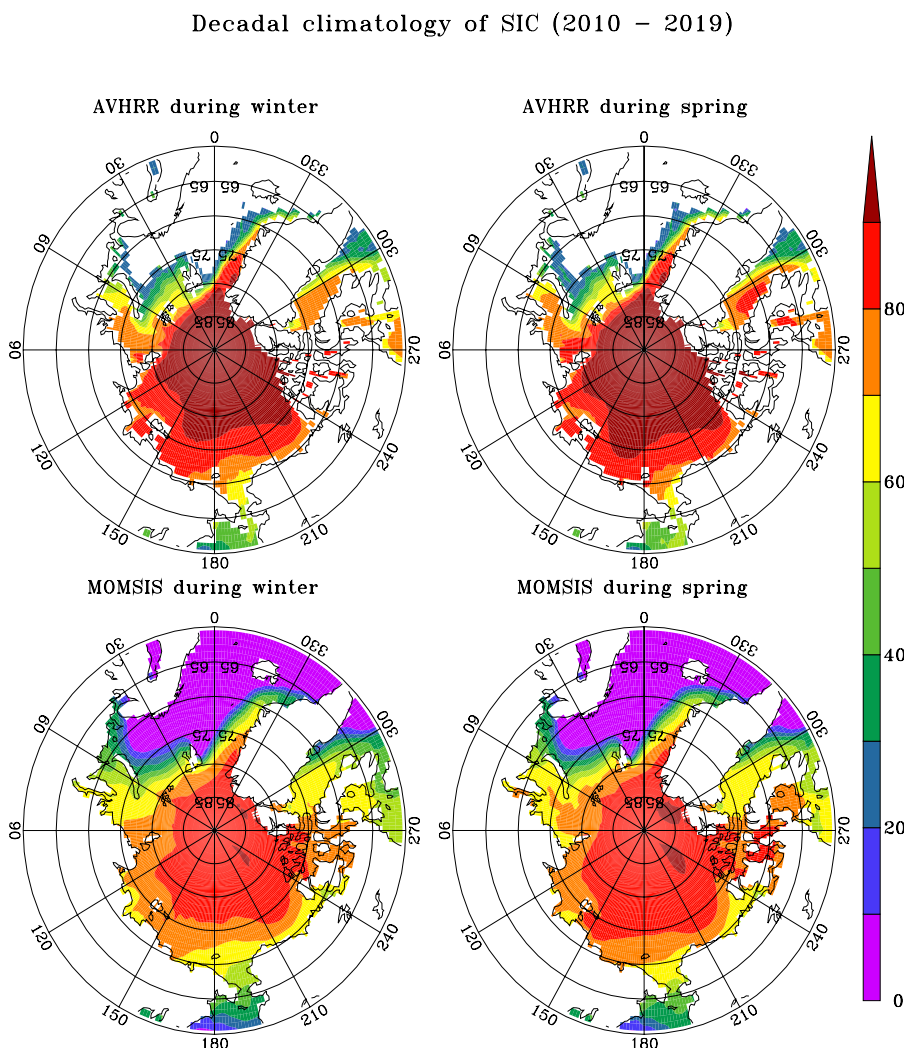
AVHRR data shows similar maximum decadal reduction of SIC during summer and autumn seasons in the Barents (part of S02), Kara (part of S03) and Laptev (part of S04) Sea regions of the Arctic as observed during other seasons (Fig. 8). MOMSIS also shows similar maximum decadal reduction of SIC in all above three regions of the Arctic during summer and autumn seasons. As an example in the Barents Sea (part of S02) regions, AVHRR shows average decadal change of SIC with -2.27% and -3.23% during summer and autumn seasons respectively. MOMSIS also shows similar decadal change of SIC in Barents (part of S02) Sea regions with -4.94% and -5.93% during above seasons (Table 4).

MOMSIS also successfully simulates AVHRR observed very small decadal change of SIC in the western Arctic

regions which includes Beaufort (part of S07) and Chukchi (part of S06) Sea regions during all four seasons. As discussed above, small decadal change of SIC in above regions leads to below 90% statistical significance level. As an example, in the Beaufort (part of S07) Sea regions of the Arctic, AVHRR shows decadal change of -0.21%, -0.22%, -1.66% and -2.41% during winter, spring, summer and autumn seasons respectively (Table 4). MOMSIS also shows smaller, but higher than AVHRR with decadal decrease of -3.20%, -1.20%, -3.68% and -5.80% during above seasons respectively. Only in the Greenland Sea, AVHRR shows small decadal increase of SIC during all four seasons (Table 4). However, MOMSIS shows very small decadal decrease of SIC instead of any decadal increase in the Greenland Sea during all four seasons (Figs. 7, 8 and Table 4).

During winter and spring seasons in the Arctic, AVHRR also showed maximum decadal increase of SST in the Barents (part of S02), Kara (part of S03) and Laptev (part of S04) Sea regions of the Arctic (Fig. 9). MOMSIS also successfully simulates maximum decadal increase of SST during winter and spring seasons in above regions. As an

**Fig. 3** Figure shows comparison of decadal climatology of SIC (%) in the Arctic between AVHRR and MOMSIS during winter (left two panels) and spring seasons (right two panels). Decadal climatology is estimated by removing annual variability from SIC using 400 days low-pass fourth order time series Butterworth filter



example in the Barents (part of S02) Sea regions, AVHRR shows average decadal increase of SST with  $0.54\text{ }^{\circ}\text{C}$  and  $0.41\text{ }^{\circ}\text{C}$  during winter and spring seasons respectively. MOMSIS also shows similar decadal SST increase of  $0.54\text{ }^{\circ}\text{C}$  and  $0.37\text{ }^{\circ}\text{C}$  during above seasons in above regions. Similarly, best performance of MOMSIS are also observed in simulation of AVHRR observed maximum decadal increase of SST in Barents (part of S02), Kara (part of S03) and Laptev (part of S04) Sea regions of the Arctic during summer and autumn seasons (Fig. 10). As an example, in the Barents (part of S02) Sea regions, AVHRR showed average decadal SST increase of  $0.56\text{ }^{\circ}\text{C}$  and  $0.64\text{ }^{\circ}\text{C}$  during summer and autumn seasons (Table 4). MOMSIS also shows similar results with decadal SST increase of  $0.51\text{ }^{\circ}\text{C}$  and  $0.64\text{ }^{\circ}\text{C}$  during above seasons in above regions (Table 4).

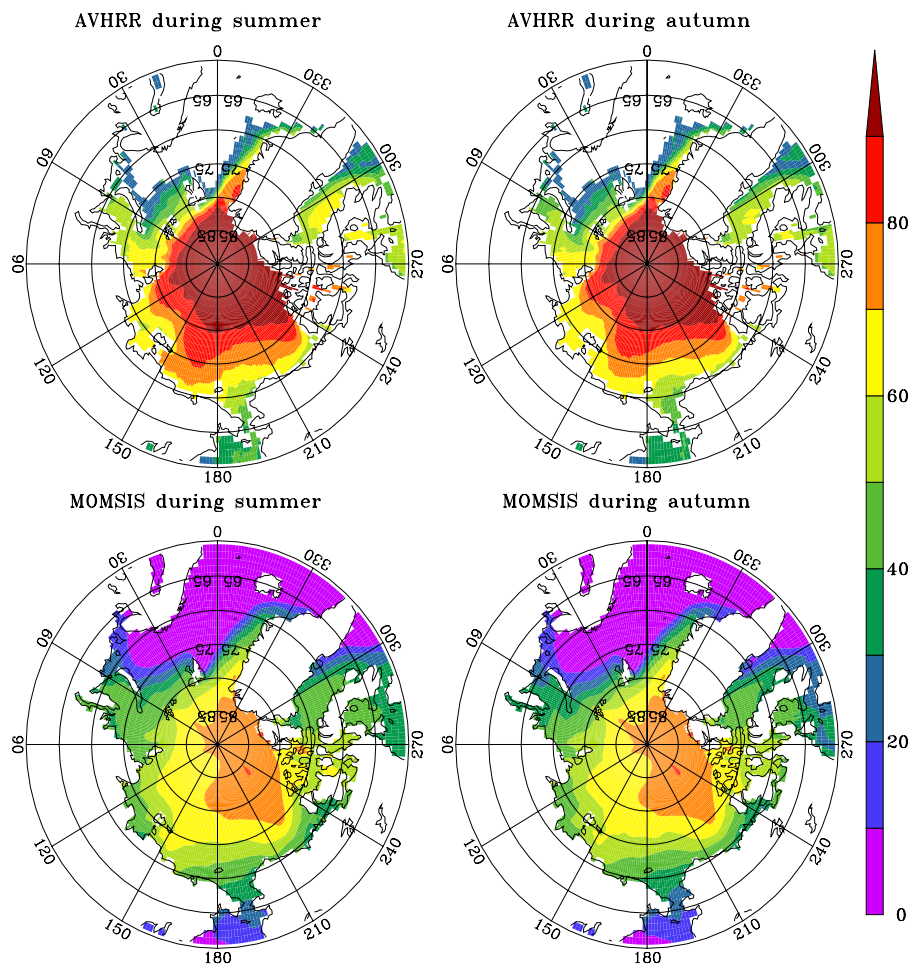
It has been observed that MOMSIS successfully simulates small average AVHRR observed decadal increase of SST in the Greenland (part of S08) Sea regions, however, it was opposite for SIC (Table 4). For SST decadal change

also, best performance of MOMSIS are restricted south of  $80^{\circ}\text{ N}$ . In conclusion, it can be confirmed that MOMSIS perform very well in simulation of AVHRR observed decadal change of SIC and SST in the Arctic during all four seasons (winter, spring, summer and autumn) except very few occasions and also in the south of  $80^{\circ}\text{ N}$ . At higher latitudes (north of  $80^{\circ}\text{ N}$ ), the performance of MOMSIS decreases and need to be improved. Also, it is important to note that the performance of MOMSIS are slightly better in simulation of AVHRR observed decadal change of SST in the Arctic compared to SIC.



**Fig. 4** Similar like Fig. 3, but during summer (left two panels) and autumn seasons (right two panels)

Decadal climatology of SIC (2010 – 2019)



**5 Upper ocean heat budget analysis for decadal change of SST and SIC in the Arctic**

In order to understand significance of thermodynamics processes associated with decadal change of SIC and SST during all four seasons of the Arctic, an upper ocean heat budget analysis has been performed in the Arctic ocean (Vialard and Delecluse 1998; Chen et al. 2015; Vijith et al. 2020).

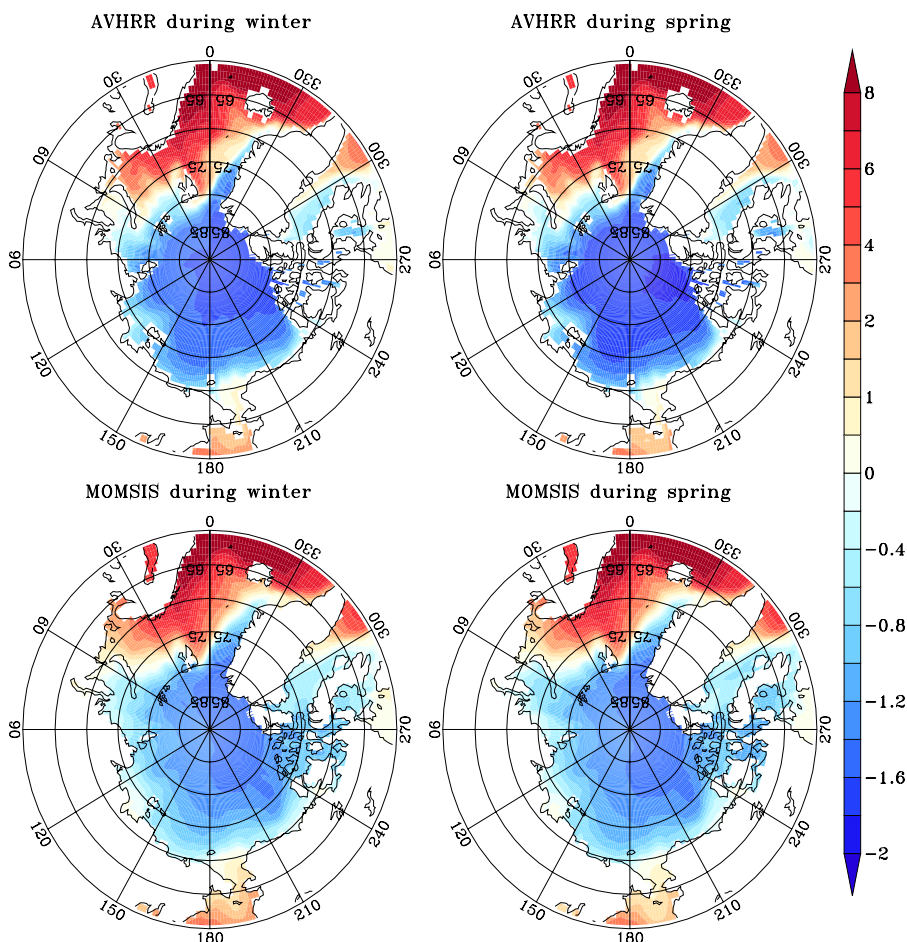
The equations for heat budget is as follows

$$\partial_t T_{ML} = \underbrace{\frac{(Q_{loss} + \sum_{-h}^0 Q_{abs})}{\rho_o C_p h}}_{\text{Net Atmospheric heatfluxes}} + \underbrace{\frac{-1}{h} \left( \int_{-h}^0 u \partial_x T dz + \int_{-h}^0 v \partial_y T dz \right)}_{\text{Horizontal advection}} + \underbrace{\frac{1}{h} [w_{-h} (T_{-h} - T_{ML})]}_{\text{Vertical advection}} + \text{Residual.} \tag{2}$$

In equations,  $T$ ,  $h$ ,  $u$ ,  $v$ ,  $w$ ,  $\rho_o$  (fixed value of  $1035.00 \text{ kg m}^{-3}$ ) and  $C_p$  (fixed value of  $3989.24 \text{ J kg}^{-1} \text{ K}^{-1}$ ) are the potential temperature, Mixed Layer Depth (MLD), zonal velocity, meridional velocity, vertical velocity, density of water and specific heat capacity, respectively.  $\partial_t T_{ML}$  represents rate of Mixed Layer Temperature, defined as MLT rate.  $Q_{loss}$  is the heat loss from the surface as turbulent and long-wave fluxes.  $Q_{abs}$  is the shortwave radiation absorbed by Seawater.  $T_{-h}$  and  $w_{-h}$  represents water temperature and vertical velocity at the base of MLD. Residual term in the Eq. 2 represents heat loss due to ocean vertical processes other than vertical advection and ocean internal variability. In this manuscript, combination of horizontal and vertical advection term is used as a ocean advection component in order to quantify the role of ocean advection on decadal change of SST and SIC. Annual mean has been removed from each components of the heat budget term by using 400 days low-pass 4<sup>th</sup> order Butterworth time-series filter.

Statistical student t-test for four component of heat budget term (MLT rate, net atmospheric heat (NAH) flux, Ocean

**Fig. 5** Comparison of decadal climatology of SST ( $^{\circ}\text{C}$ ) in the Arctic between AVHRR and MOMSIS during winter (left two panels) and spring seasons (right two panels). Decadal climatology is estimated by removing annual variability from SST using 400 days low-pass fourth order Butterworth filter



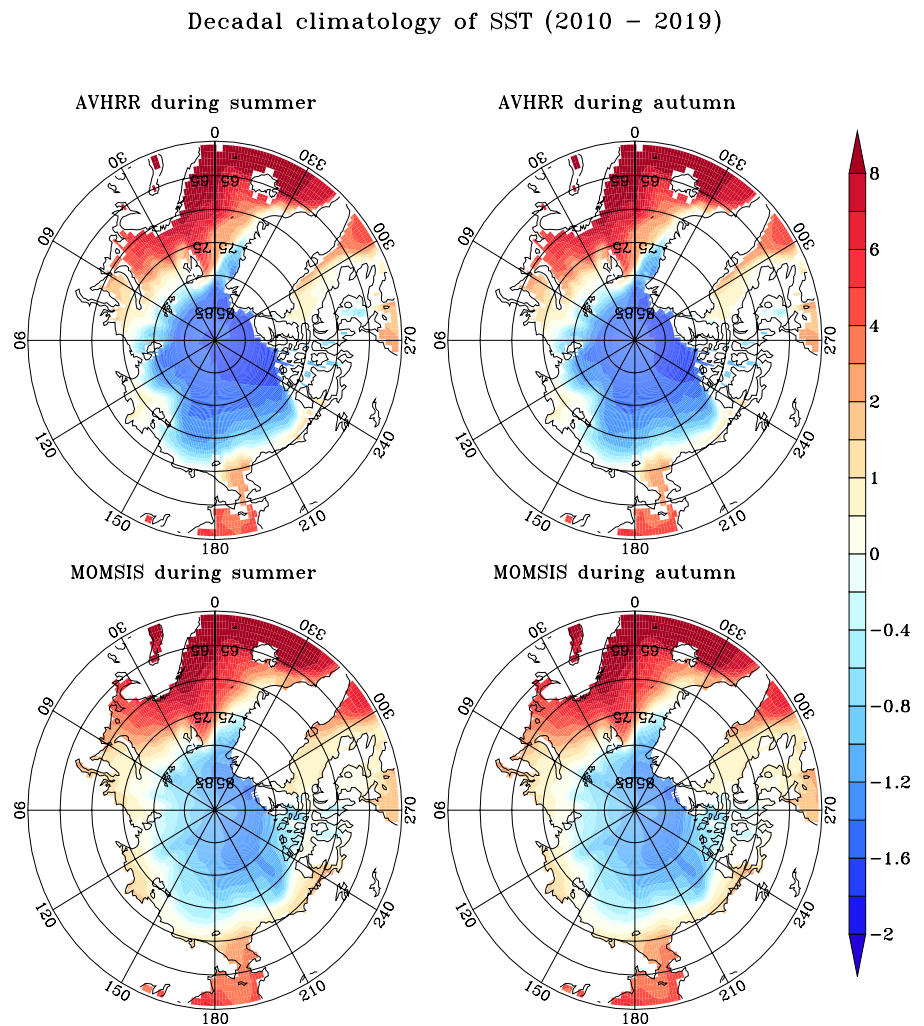
advection and Residual processes) has been performed to quantify 90% significance level related to decadal change between two decade (2000–2009 and 2010–2019). Detailed procedure of t-test has been described in Sect. 2.4. Very low t-value at all eight sectors of Arctic for MLT rate imply no 90% statistical significance for decadal change (Table 2). Similarly, no 90% statistical significance has been observed for decadal change of SST rate using both AVHRR and MOMSIS (Table 2). MOMSIS shows 90% statistical significance for NAH flux only at Barents (part of S02), Kara (part of S03), Laptev (part of S04) and Beaufort (part of S07) Sea regions. However, using AVHRR, no 90% statistical significance has been observed for both SIC and SST decadal change at Beaufort (part of S07) Sea regions. Similar with NAH flux, lower t-value has been observed for residual processes along-with 90% statistical significant at Barents (part of S02), Kara (part of S03) and Laptev (part of S04) Sea regions. Interestingly, for ocean advection, 90% statistical significance has been observed for 06 major sectors excluding Chukchi Sea (part of S06) and Greenland Sea (part of S08). Also, higher t-value associated with ocean advection has been observed for Barents (part of S02), Kara (part of S03) and Laptev (part of S04) Sea regions, where maximum

decadal change of SIC and SST has been observed. Also, in the Beaufort Sea (part of S07), where decadal change of both SIC and SST are small, ocean advection is 90% statistical significant. This further imply that ocean advection has a critical role for smaller decadal change of SIC and SST along-with NAH fluxes in the Beaufort (part of S07) Sea regions.

### 5.1 Winter seasons

Heat budget analysis using MOMSIS shows prominent decadal change in rate of MLT during all four seasons, which includes winter, spring, summer and autumn (Fig. 11). During winter seasons, maximum decadal change of MLT rate has been observed in the Barents (part of S02), Kara (part of S03) and Laptev (part of S04) Sea regions of the Arctic (defined as S02, S03 and S04) (Figs. 11 and 12). Negative decadal MLT rate change has been observed during winter seasons due to decrease of decadal SST during months of winter seasons, which includes December, January and February (figure not shown). Both, AVHRR and MOMSIS also showed decadal increase of SST in above regions; higher

**Fig. 6** Similar like Fig. 5, but during summer (left two panels) and autumn seasons (right two panels)



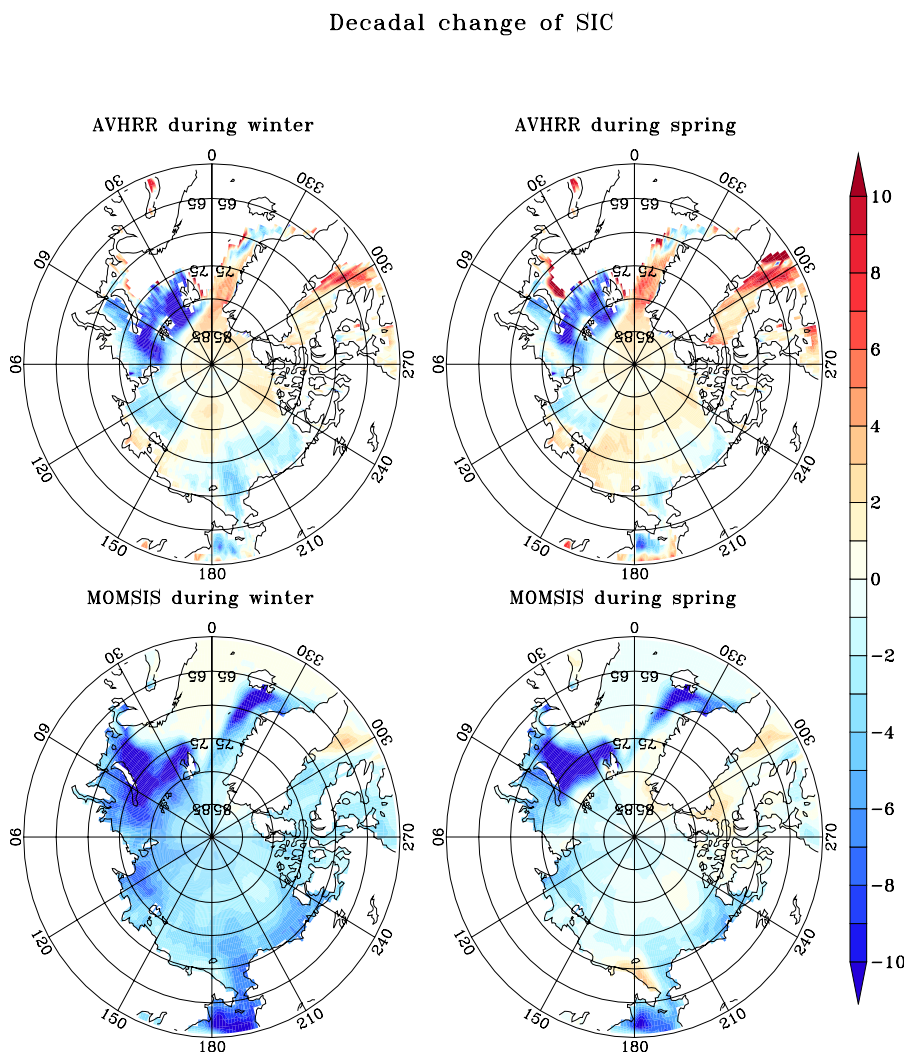
SST during winter seasons in above regions during decade of 2010–2019 compared to 2000–2009 (Fig. 9).

Decadal decrease of SST rate (Figure S7) and decadal increase of SST in above regions during winter seasons imply that decrease rate of MLT during winter months for 2010–2019 decade is much higher compared to 2000–2009 (SST increased for 2010–2019 decade during months of winter seasons compared to 2000–2009). As an example, in the Barents (part of S02) Sea for 2000–2009 decade, average SST rate (SST value) of  $-0.26\text{ }^{\circ}\text{C month}^{-1}$  ( $0.42\text{ }^{\circ}\text{C}$ ) are observed for winter seasons with  $-0.30\text{ }^{\circ}\text{C month}^{-1}$ ,  $-0.29\text{ }^{\circ}\text{C month}^{-1}$  and  $-0.13\text{ }^{\circ}\text{C month}^{-1}$  ( $0.78\text{ }^{\circ}\text{C}$ ,  $0.12\text{ }^{\circ}\text{C}$  and  $-0.05\text{ }^{\circ}\text{C}$ ) for December, January and February months respectively. Similarly, in the Barents Sea for 2010–2019 decade, average SST rate (SST value) of  $-0.29\text{ }^{\circ}\text{C month}^{-1}$  ( $0.95\text{ }^{\circ}\text{C}$ ) is observed for winter seasons with  $-0.35\text{ }^{\circ}\text{C month}^{-1}$ ,  $-0.32\text{ }^{\circ}\text{C month}^{-1}$  and  $-0.13\text{ }^{\circ}\text{C month}^{-1}$  ( $1.35\text{ }^{\circ}\text{C}$ ,  $0.70\text{ }^{\circ}\text{C}$  and  $0.40\text{ }^{\circ}\text{C}$ ) for December, January and February months respectively.

Negative SST trend from December to February seasons also can be interpreted as increase of SST from February to December month via backward integration. So, decrease of decadal SST rate for 2010–2019 compared to 2000–2009 further imply increase of decadal SST from February to December in reverse ways. So, in conclusion, negative decadal MLT rate change during winter and also during autumn seasons can be interpreted in reverse ways to relate it with increase of SST from February to December and also, during November to September. Detailed validation of SST rate for decadal climatology and decadal change between AVHRR and MOMSIS has been included in the supplementary documents (Figures S5, S6, S7 and S8). However, due to increase of SST during spring (March–May) and summer season months (June–August), decadal increase of MLD rate during above seasons can be interpreted using forward integration from the month of March to August.

During winter seasons, decadal reduction of MLT rate at Barents (part of S02), Kara (part of S03) and Laptev (part of S04) Sea regions of the Arctic are dominated by decadal

**Fig. 7** Comparison of decadal change of SIC in the Arctic between AVHRR and MOMSIS during winter (left two panels) and spring seasons (right two panels). The unit of SIC is %. Decadal change is estimated by subtracting decadal climatology between 2010–2019 and 2000–2009

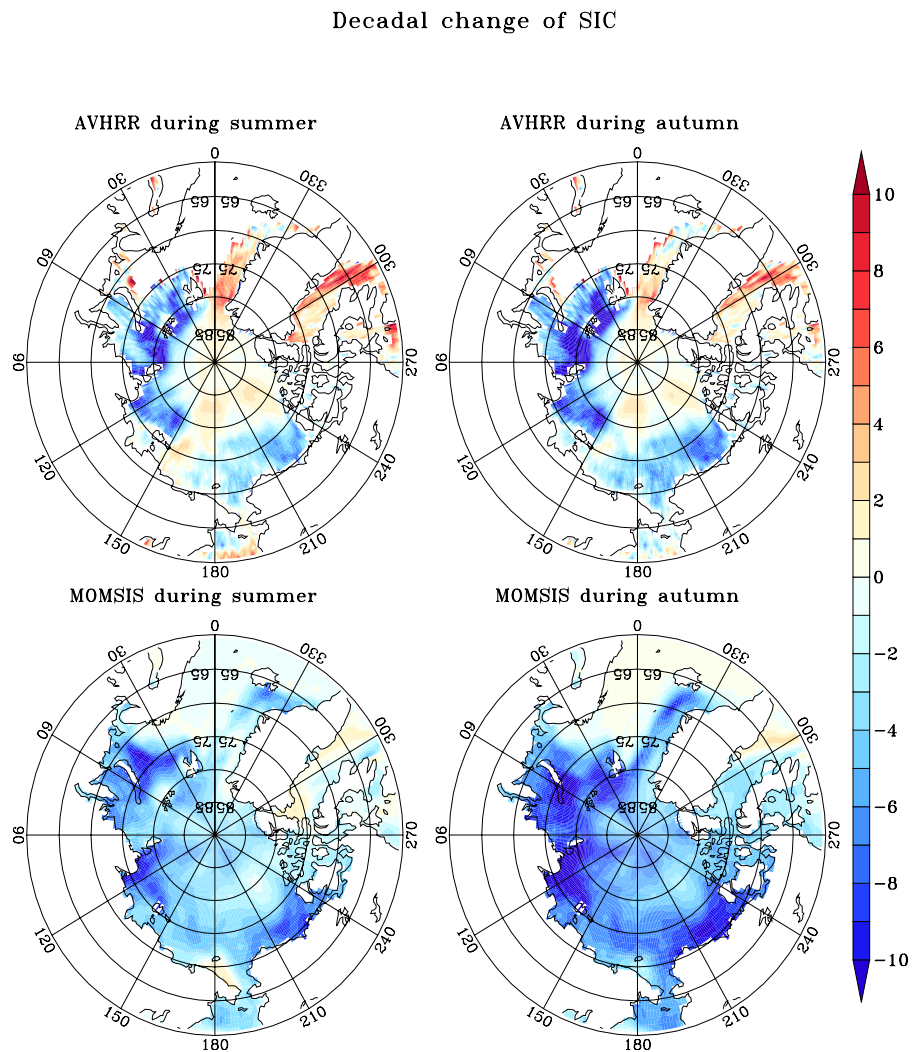


decrease of net atmospheric heat (NAH) fluxes (Figs. 11 and 12). MOMSIS shows dominance of ocean advection during winter seasons only in the Norwegian (part of S01) and Beaufort (part of S07) Sea regions. In above sea regions during winter seasons, ocean advection play most significant role compared to NAH fluxes for decadal change of MLT rate. As an example in the Norwegian Sea, average decadal change of MLT rate during winter seasons is  $-0.02\text{ }^{\circ}\text{C month}^{-1}$ , which is dominated by decadal change of ocean advection with average value of  $-0.02\text{ }^{\circ}\text{C month}^{-1}$  (Fig. 11). As a part of ocean advection, horizontal advection dominate compared to vertical advection during winter seasons (Fig. 13). Very small and negligible contribution of vertical advection has been observed compared to horizontal at all eight sectors of the Arctic. In other sea regions of the Arctic during winter seasons, decadal change of MLT rate are dominated by NAH fluxes and residual processes.

## 5.2 Spring seasons

Positive decadal change of MLT rate has been observed during spring seasons with its maximum strength at Barents (part of S02), Kara (part of S03) and Laptev Sea (part of S04) regions of the Arctic (Figs. 10 and 12). During spring seasons, MLD rate is positive almost in the entire Arctic except few regions due to increase of SST during spring season months, which includes March, April and May (figure not shown). As an example, in the Barents Sea (part of S02), MOMSIS shows  $0.04\text{ }^{\circ}\text{C month}^{-1}$  decadal change of MLT rate during spring seasons, which are dominated by decadal change of NAH fluxes ( $0.11\text{ }^{\circ}\text{C month}^{-1}$ ) and residual processes ( $-0.09\text{ }^{\circ}\text{C month}^{-1}$ ). MOMSIS also showed maximum strength of ocean advection in the Norwegian (part of S01) and Beaufort Sea (part of S07) regions of the Arctic during spring seasons. In the Norwegian Sea (part of S01), small negative decadal change of SST rate during spring seasons are dominated by destructive interference between positive decadal change of net heat fluxes and negative decadal

**Fig. 8** Similar like Fig. 7, but during summer (left two panels) and autumn seasons (right two panels)

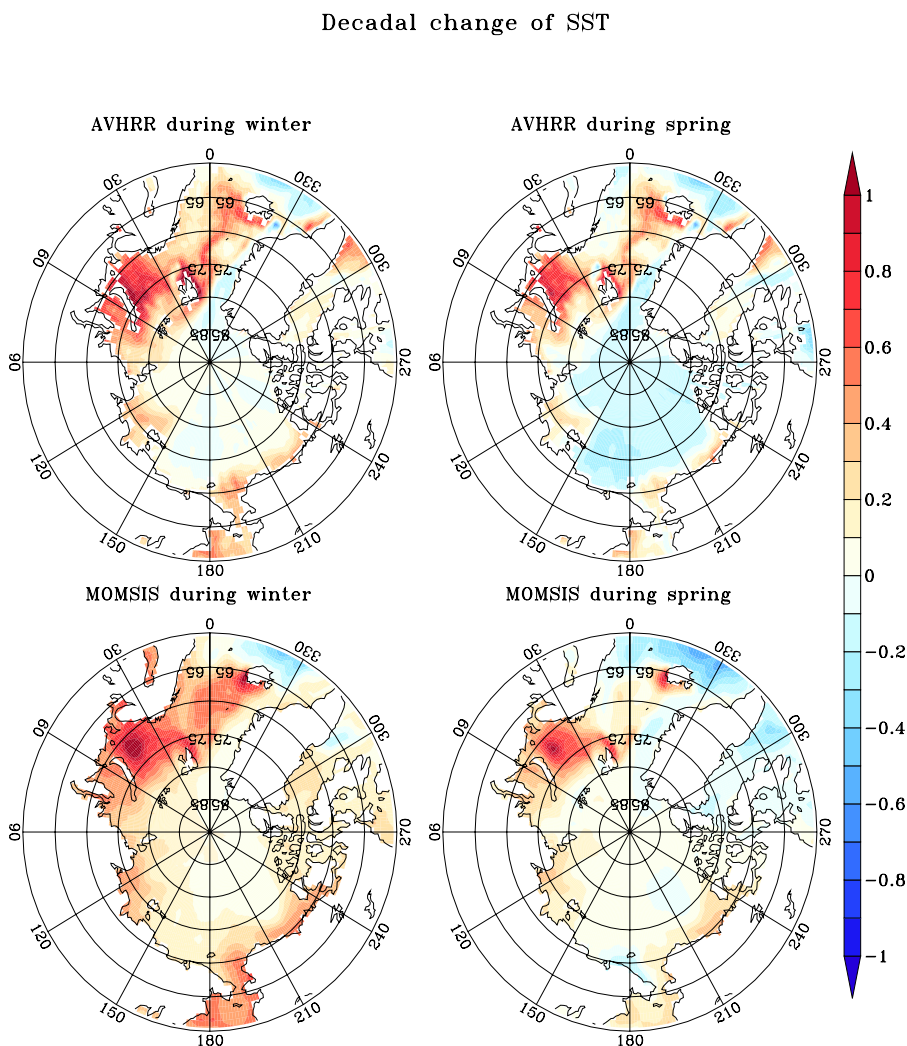


change of ocean advection (Fig. 11). However, in the Beaufort Sea (part of S07), small positive decadal change of MLT rate during spring seasons are dominated by destructive interference between positive decadal change of NAH fluxes and negative decadal change of ocean advection along with ocean residual processes. Due to strong dominance of destructive interference between decadal change of NAH fluxes and ocean advection, very small decadal increase of SST and decrease of SIC has been observed in the Norwegian (part of S01) and Beaufort (part of S07) Sea regions of the Arctic. Similar like winter seasons, very small and negligible contribution of vertical advection has been observed during spring seasons compared to ocean horizontal advection in all eight sectors of the Arctic (Fig. 13). In other sea regions of the Arctic during spring seasons which includes East Siberian (part of S05) and Chukchi (part of S06) Sea regions, small decadal change of MLT rate are observed due to small decadal change of NAH fluxes and residual processes (Figs. 11 and 12).

### 5.3 Summer seasons

During summer seasons in the Arctic, maximum positive decadal change of MLT rate also has been observed in the Barents (part of S02), Kara (part of S03) and Laptev (part of S04) Sea regions of the Arctic (Figs. 11 and 12). Similar like spring seasons, positive rate of MLT has been observed almost in the entire Arctic except few regions due to increase of SST during summer season months, which includes June, July and August (figure not shown). As an example in the Barents Sea (part of S02), MOMSIS shows  $0.03\text{ }^{\circ}\text{C month}^{-1}$  decadal change of MLT rate during spring seasons, which are dominated by decadal change of NAH fluxes ( $0.12\text{ }^{\circ}\text{C month}^{-1}$ ) and residual processes ( $-0.10\text{ }^{\circ}\text{C month}^{-1}$ ). Similar with winter and spring seasons, maximum decadal change of ocean advection with dominance of horizontal advection compared to vertical has been observed in the Norwegian (part of S01) and Beaufort Sea (part of S07) regions of the Arctic during summer seasons. In both Norwegian (part of S01) and Beaufort

**Fig. 9** Comparison of decadal change of SST in the Arctic between AVHRR and MOMSIS during winter (left two panels) and spring seasons (right two panels). The unit of SST is °C. Decadal change is estimated by subtracting decadal climatology between 2010–2019 and 2000–2009



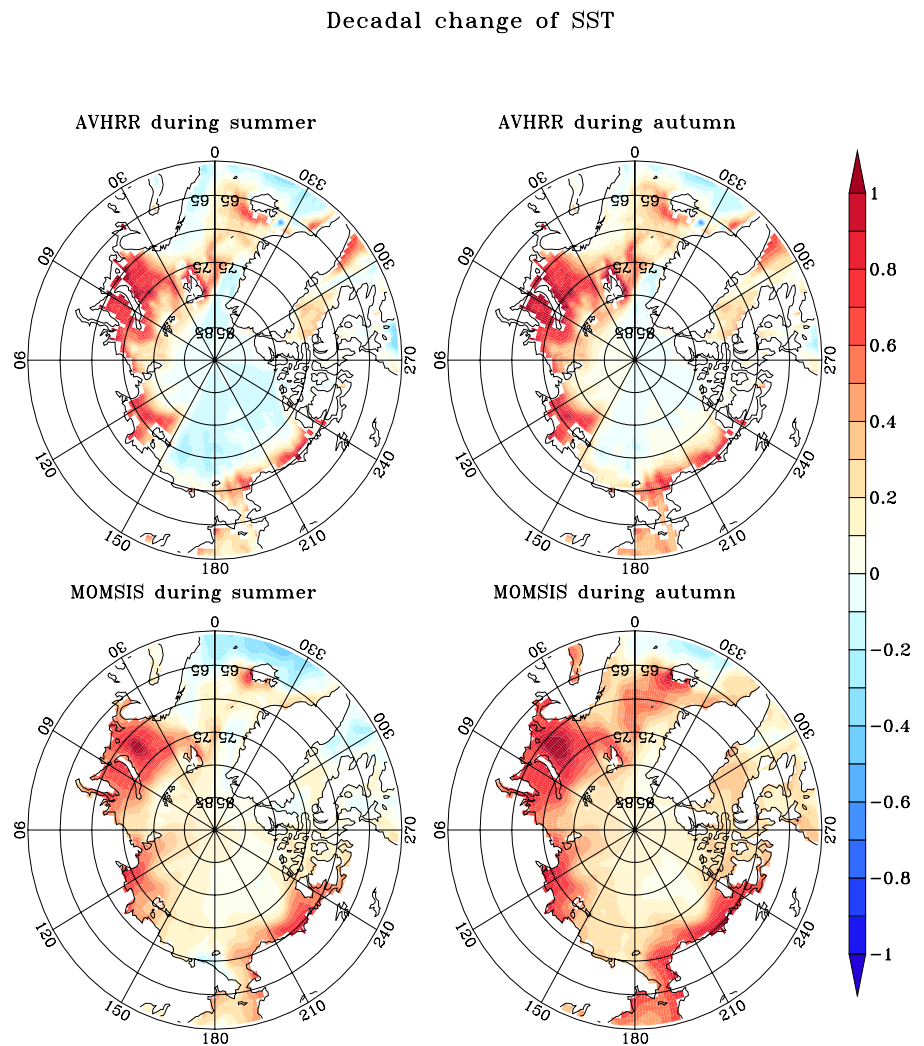
(part of S07) Sea regions, small positive decadal change of MLT rate during summer seasons are dominated by destructive interference between positive decadal change of NAH fluxes and negative decadal change of ocean advection along with ocean residual processes (Fig. 11). In other Sea regions of the Arctic during summer seasons, which includes East Siberian (part of S05) and Chukchi (part of S06) Sea regions, small decadal change of MLT rate are observed due to small decadal change of NAH fluxes and residual processes (Figs. 11 and 12).

#### 5.4 Autumn seasons

MOMSIS also showed maximum negative decadal change of MLT rate during autumn seasons in the Barents (part of S02), Kara (part of S03) and Laptev (part of S04) Sea regions of the Arctic, as similar during other three seasons (Figs. 11 and 12). However, in above three regions during autumn seasons, decadal change of MLT rate are dominated by residual processes compared to NAH fluxes and ocean advection. As

an example in the Barents (part of S02) Sea during autumn seasons, our model MOMSIS shows  $-0.03\text{ °C month}^{-1}$  decadal change of MLT rate, which are dominated by decadal change of NAH fluxes ( $-0.01\text{ °C month}^{-1}$ ) and residual processes ( $-0.02\text{ °C month}^{-1}$ ). Also, maximum decadal change of ocean advection has been observed in the Norwegian (part of S01) and Beaufort (part of S07) Sea regions of the Arctic during autumn seasons as observed during other three seasons, however, strength of decadal change of ocean advection is high in the Beaufort Sea ( $-0.06\text{ °C month}^{-1}$ ) compared to Norwegian Sea ( $-0.02\text{ °C month}^{-1}$ ). Also, contribution of decadal change of ocean horizontal advection dominate compared to vertical at all eight sectors of the Arctic during autumn seasons (Fig. 13). Similar destructive interference has been observed between decadal change of NAH fluxes and ocean advection along with residual processes in the Norwegian (part of S01) and Beaufort (part of S07) Sea regions of the Arctic during autumn seasons and are responsible for formation of small decadal change of MLT rate along with small decadal increase (decrease)

**Fig. 10** Similar like Fig. 9, but during summer (left two panels) and autumn seasons (right two panels)



of SST (SIC). Similar with other three seasons, in other sea regions of the Arctic during autumn seasons, small decadal change of MLT rate has been observed due to small decadal change of NAH fluxes and residual processes (Figs. 11 and 12).

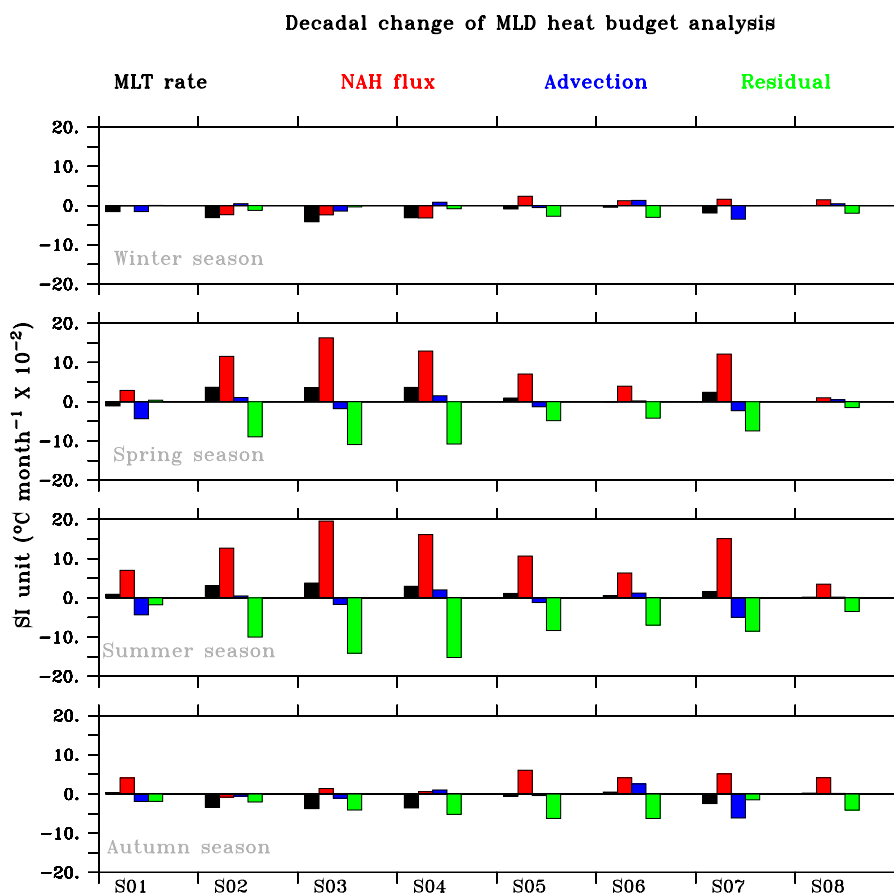
## 6 Summary and discussions

In this article, role of atmosphere net heat fluxes and ocean advection for decadal change (between decade of 2010–2019 and 2000–2009) of SIC and SST in the Arctic ( $60^{\circ}$  N– $90^{\circ}$  N) has been discussed. Our model MOMSIS successfully simulates AVHRR observed maximum decadal reduction of SIC and increase of SST in the Barents (part of S02), Kara (part of S03) and Laptev (part of S04) Sea regions during all four seasons of the Arctic; winter, spring, summer and autumn except few occasions. Also, best performance of model MOMSIS are restricted south of  $80^{\circ}$  N in the Arctic. Very small decadal reduction of SIC and increase of SST has

been observed in the Norwegian (part of S01) and Beaufort (part of S07) Sea regions of the Arctic using both AVHRR and MOMSIS. AVHRR showed statistical significance for decadal change at 06 sectors except Chukchi (part of S06) and Beaufort (part of S07) Sea. However, MOMSIS showed 90% statistical significance at all eight sectors of the Arctic.

Using upper ocean MLD heat budget analysis, it has been observed that decadal change of NAH flux play most significant role for maximum decadal decrease of SIC and increase of SST during all four seasons in the Arctic with 90% statistical significance at Kara (part of S03), Laptev (part of S04), East Siberian (part of S5) and Beaufort (part of S07) Sea regions. Maximum average decadal decrease of NAH flux has been observed in the Barents (part of S02), Kara (part of S03) and Laptev (part of S04) Sea regions of the Arctic during winter seasons and responsible for decadal decrease of MLT rate and also, increase of average SST in above regions. During summer and spring seasons, MOMSIS shows strong decadal increase of NAH fluxes in above three regions of the Arctic, which are responsible for decadal

**Fig. 11** Histogram showing decadal change of Mixed Layer Depth (MLD) heat budget analysis in the Arctic. Black, red, blue and green colour values in the each box represents Mixed Layer Temperature (MLT) rate, net atmospheric heat (NAH) flux, ocean advection and residual processes respectively as written in Eq. 2. Four panels shown in the figure represents heat budget analysis for four seasons; winter, spring, summer and autumn. Here, in the X-axis, total eight sectors named as S01, S02, S03, S04, S05, S06, S07 and S08 represents major part of Norwegian Sea, Barents Sea, Kara Sea, Laptev Sea, East Siberian Sea, Chukchi Sea, Beaufort Sea and Greenland Sea respectively and described at Table 1. The Y-axis represents unit of all four heat budget terms in the SI unit ( $^{\circ}\text{C month}^{-1}$ )



increase of average SST rate and increase of average SST. During autumn seasons, MOMSIS shows strong decadal decrease of residual processes compared to decadal increase of NAH fluxes in above three regions of the Arctic and are responsible for decadal decrease of average MLT rate and increase of average SST.

Using MLD heat budget analysis of upper ocean, it has been observed that destructive interference between decadal change of NAH fluxes and ocean advection play most crucial role for very small decadal decrease of SIC and increase of SST in the Norwegian (part of S01) and Beaufort (part of S07) Sea regions of the Arctic. At Norwegian Sea (part of S01), only decadal change of ocean advection is 90% statistical significance. However, at Beaufort (part of S07) Sea, both NAH fluxes and ocean advection are at 90% statistical significance level.

In the Norwegian (part of S01) Sea, during winter seasons, small decadal decrease of MLT rate, SIC and increase of SST are significantly controlled by small decadal decrease of ocean advection. During other seasons, decadal change of MLT rate are very small compared to winter. Strong destructive interference between negative decadal change of ocean advection and positive decadal change for NAH fluxes play an important role for very small decadal change of MLT

rate, SST and SIC in the Norwegian (part of S01) Sea during spring, summer and autumn seasons. In the Beaufort (part of S07) Sea regions of the Arctic during all four seasons, strong destructive interference between positive decadal change of NAH fluxes and negative ocean advection along with negative residual process are observed, which are responsible for small decadal increase of SST and decadal decrease of SIC.

It is known from earlier research that Norwegian (part of S01) Sea regions are the major pathways for intrusion of warmer Atlantic water in the Arctic (Pickart and Spall 2007; Muilwijk et al. 2018; Kim and Kim 2019; Wang et al. 2020; Smedsrud et al. 2021). Similarly, Beaufort (part of S02) Sea regions are the major pathways for intrusion of warmer Pacific water in the Arctic (Proshutinsky et al. 2002; Chatterjee et al. 2018; Amritage et al. 2020). Using MLD heat budget analysis, similar strong decadal change of ocean advection has been observed in the Norwegian (part of S01) and Beaufort (part of S02) Sea regions of the Arctic during all four seasons. Strong decadal decrease of ocean advection in the above two sectors play an important role for small decadal decrease of SIC and increase of SST in above two sectors compared to other sectors in the Arctic during all four seasons. MOMSIS also shows small decadal increase of ocean advection in the Barents (part of S02), Laptev (part



**Fig. 12** Decadal change of MLD heat budget analysis for winter (first column), spring (second column), summer (third column) and winter (fourth column). First row of the column shows decadal change of Mixed Layer Temperature (MLT) rate ( $^{\circ}\text{C month}^{-1}$ ), second row shows decadal change of net atmospheric heat (NAH) flux ( $^{\circ}\text{C month}^{-1}$ ) and ocean advection ( $^{\circ}\text{C month}^{-1}$ ) and fourth row shows decadal change of residual processes ( $^{\circ}\text{C month}^{-1}$ )

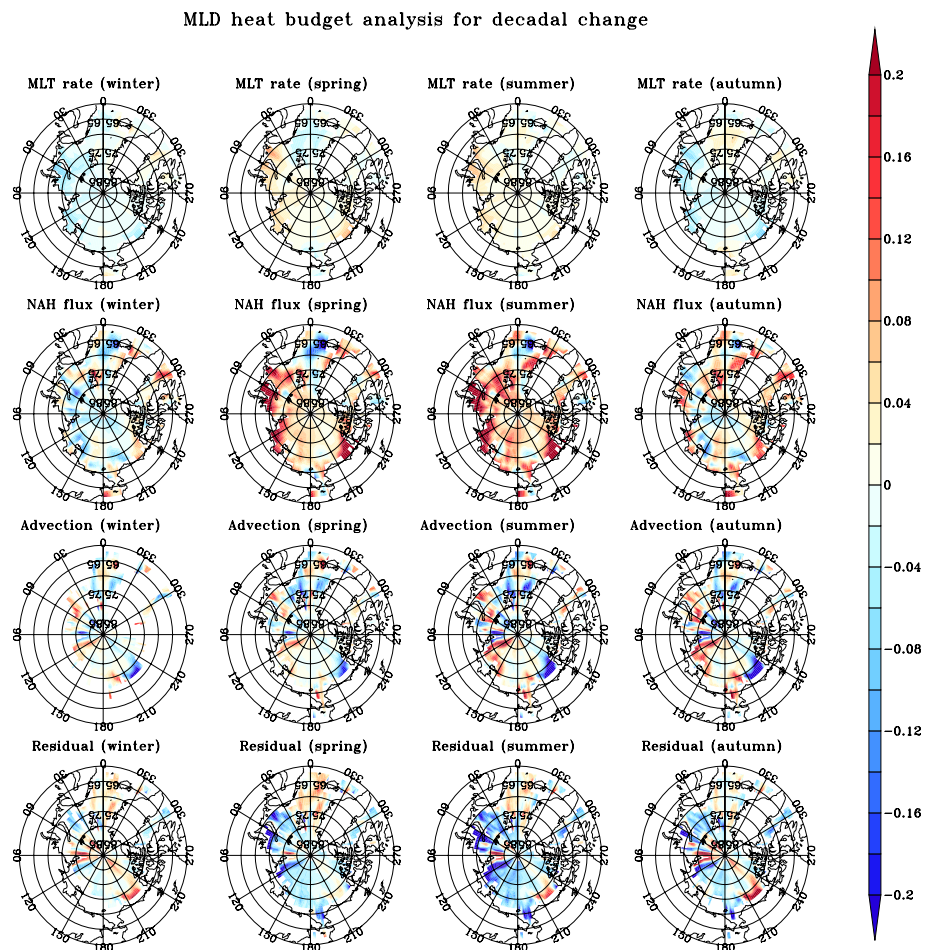
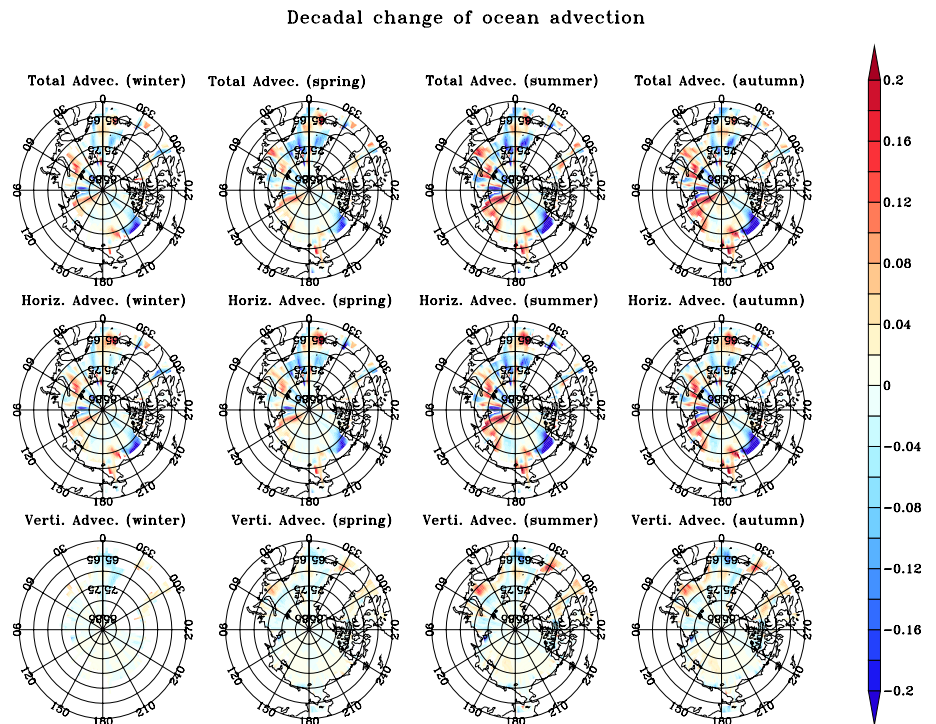


**Fig. 13** Decadal change of ocean advection for winter (first column), spring (second column), summer (third column) and winter (fourth column) seasons. First row of the column shows decadal change of net ocean advection ( $^{\circ}\text{C month}^{-1}$ ), second row shows decadal change of horizontal ocean advection ( $^{\circ}\text{C month}^{-1}$ ) and third row shows decadal change of vertical advection ( $^{\circ}\text{C month}^{-1}$ )



of S04) and Chukchi (part of S06) Sea regions of the Arctic during all seasons, however, decadal change of SIC and SST in above regions are dominated by decadal change of NAH fluxes and other residual processes. MOMSIS also shows that decadal change of ocean advection are strongly dominated by its spatial variations. Similar spatial variations also observed for decadal change of NAH fluxes. Also, horizontal ocean advection dominate compared to vertical in terms of ocean advection contribution for decadal change of SIC and SST. Very small and negligible decadal change of vertical advection has been observed along all eight sectors of the Arctic during all four seasons.

It has been observed that best of performance of MOMSIS in simulating AVHRR observed decadal change of SIC and SST are restricted between 60° N–80° N. At higher latitude (north of 80° N), AVHRR shows smaller decadal increase of SIC and decrease of SST, however, smaller opposite decadal change has been observed for both SIC and SST using MOMSIS. Also, in the Greenland (part of S08) Sea regions, MOMSIS showed small decadal decrease of SIC and increase of SST compared to AVHRR observed small decadal increase of SIC and decrease of SST. Another major problem of MOMSIS are related to warmer bias for SST and smaller bias for SIC during summer and autumn seasons, when sea-ice start to melt and new sea-ice start to form. One possible reason can be related to atmospheric forcing using ERA5, whose performance on MOMSIS can be validated with any other atmospheric forcing from global reanalysis atmospheric or earth system models. Another possible reason can be associated with horizontal resolution of both ocean and sea-ice model, which need to be improved. Also, ocean and sea-ice parametrization need to be revised in order to improve the performance of the model in the polar regions.

In this article, results are restricted on decadal variability of SIC and SST during four seasons in the Arctic and possible role of decadal change of atmospheric net heat fluxes and ocean advection on it. Detailed study related to decadal change of possible pathways of ocean advection and inclusion of warmer Atlantic and Pacific water in the Arctic need to be investigated in future.

**Supplementary Information** The online version contains supplementary material available at <https://doi.org/10.1007/s00382-022-06531-7>.

**Acknowledgements** The authors acknowledge Ministry of Earth Sciences (MoES), Government of India and National Centre for Polar and Ocean Research (NCPOR) for their support. Our special thanks to Dr. Abhisek Chatterjee and Mrs. Purna Singh from Indian National Centre for Ocean Information Services (INCOIS), MoES, Hyderabad, India for their help in model set-up. Model simulations are carried out at “Pratush” high performance computing installed at Indian Institute of Tropical Meteorology (IITM), Pune. Ferret software has been used for analysis and plotting in the manuscript. The contribution number from NCPOR is J-40/2022-23.

**Funding** No funding has been disclosed by authors.

**Data Availability** AVHRR data has been downloaded from <https://www.ncei.noaa.gov/thredds/catalog.html>. ERA5 forcing data has been downloaded from <https://cds.climate.copernicus.eu>. Model output of MOMSIS developed at NCPOR, MoES will be available on request.

## Declarations

**Conflict of interest** Both authors declare that they have no conflict of interest.

## References

- Aksenov Y, Karcher M, Proshutinsky A, Gerdes R, Cuevas B, Golubeva E, Kauker F, Nguyen AT, Platov GA, Wadley M, Watanabe E, Coward AC, Nurser G (2016) Arctic pathways of Pacific Water: Arctic Ocean Model Intercomparison experiments. *J Geophys Res Oceans* 121:27–59. <https://doi.org/10.1002/2015JC011299>
- Amritage TWK, Manucharyan GE, Petty AA, Kwok R, Thompson AF (2020) Enhanced eddy activity in the Beaufort Gyre in response to sea ice loss. *Nat Commun* 11:761. <https://doi.org/10.1038/s41467-020-14449-z>
- Asbjornsen H, Arthun M, Skagseth O, Eldevik T (2019) Mechanisms of ocean heat anomalies in the Norwegian Sea. *J Geophys Res Oceans* 124:2908–2923. <https://doi.org/10.1029/2018JC014649>
- Bonan DB, Lehner F, Holland MM (2021) Partitioning uncertainty in projections of Arctic sea ice. *Environ Res Lett* 16(4):044002. <https://doi.org/10.1088/1748-9326/abe0ec>
- Bore GJ, Yu B (2003) Dynamical aspects of climate sensitivity. *Geophys Res Lett* 30(3):1135. <https://doi.org/10.1029/2002GL016549>
- Box J, Colgan W, Christensen TR, Schmidt N, Lund M, Parmentier F, Brown R, Bhatt U, Euskirchen E, Romanovsky V, Walsh J, Overland J, Wang M, Corell R, Meier W, Wouters B, Mernild S, Mård J, Pawlak J, Olsen M (2019) Key indicators of arctic climate change: 1971–2017. *Environ Res Lett* 14:045010. <https://doi.org/10.1088/1748-9326/aafc1b>
- Budikova D (2009) Role of Arctic sea ice in global atmospheric circulation: a review. *Glob Planet Change* 68:149–163. <https://doi.org/10.1016/j.gloplacha.2009.04.001>
- Cao Y, Bian L, Zhao J (2018) Impacts of changes in sea ice and heat flux on Arctic warming. *Atmos Clim Sci* 9:84–99. <https://doi.org/10.4236/acs.2019.91006>
- Carmack E, Polyako I, Padman L, Fer I, Hunke E, Hutchings J, Jackson J, Kelley D, Kwok R, Layton C, Melling H, Perovich D, Persson O, Ruddic B, Timmermans ML, Toole J, Ross T, Vavrus S, Winsor P (2015) Toward quantifying the increasing role of oceanic heat in sea ice loss in the new Arctic. *Bull Am Meteorol Soc* 96:150203142711003. <https://doi.org/10.1175/BAMS-D-13-00177.1>
- Chatterjee A, Shankar D, Shenoi SSC, Reddy GV, Michael GS, Ravichandran M, Gopalkrishna VV, Rao EPR, Bhaskar TVSU, Sanjeevan VN (2012) A new atlas for temperature and salinity for north Indian Ocean. *J Earth Syst Sci* 121:559–593. <https://doi.org/10.1007/s12040-012-0191-9>
- Chatterjee S, Raj RP, Bertino L, Skagseth O, Ravichandran M, Jonannesen OM (2018) Role of Greenland Sea gyre circulation on Atlantic water temperature variability in the Fram Strait. *Geophys Res Lett* 45:8399–8406. <https://doi.org/10.1029/2018GL079174>
- Chen K, Gawarkiewicz G, Kwon Y, Zhang G (2015) The role of atmospheric forcing versus ocean advection during the extreme warming

- of the Northeast U.S. continental shelf in 2012. *J Geophys Res Oceans* 120:4324–4339. <https://doi.org/10.1002/2014JC010547>
- Cheng J, Zhang S, Liu W, Dong L, Liu P, Li H (2016) Reduced interdecadal variability of Atlantic Meridional Overturning Circulation under global warming. *Proc Natl Acad Sci* 113(12):3175–3178. <https://doi.org/10.1073/pnas.1519827113>
- Comiso JC, Meier WN, Gersten R (2017) Variability and trends in the Arctic Sea ice cover: results from different techniques. *J Geophys Res Oceans* 122:6883–6900. <https://doi.org/10.1002/2017JC012768>
- Delworth TL, Broccoli AJ, Rosati A, Stouffer RJ, Balaji V, Beesley JA et al (2006) GFDL's CM2 global coupled climate models. Part I: formulation and simulation characteristics. *J Clim* 19:643–674. <https://doi.org/10.1175/JCLI3629.1>
- Drobot S, Maslanik J, Fowler C (2006) A long-range forecast of Arctic summer sea-ice minimum extent. *Geophys Res Lett* 33:L10501. <https://doi.org/10.1029/2006GL026216>
- Dunne JP, John JG, Adcroft AJ, Griffies SM, Hallberg RW, Shevliakova E, Stouffer RJ, Cooke W, Dunne KA, Harrison MJ, Krasting JP, Malyshev SL, Milly PCD, Philipps PJ, Sentman LT, Samules BL, Spelman MJ, Winton M, Wittenberg AT, Zadeh N (2012) GFDL's ESM2 global coupled climate-carbon earth system models. Part I: physical formulation and baseline simulation characteristics. *J Clim* 25:6646–6665. <https://doi.org/10.1175/JCLI-D-11-00560.1>
- England M, Jahn A, Polvani L (2019) Nonuniform contribution of internal variability to recent Arctic sea ice loss. *J Clim* 32(13):4039–4053. <https://doi.org/10.1175/JCLI-D-18-0864.1>
- Gascard JC, Zhang J, Rafizadeh M (2019) Rapid decline of Arctic sea ice volume: causes and consequences. *Cryosphere Discuss*. <https://doi.org/10.5194/tc-2019-2>
- Griffies SM, Hallberg RW (2000) Biharmonic friction with a Smagorinsky viscosity for use in large-scale eddy-permitting ocean models. *Mon Weather Rev* 128:2935–2946. <https://doi.org/10.1175/1520-0493>
- Hansen J, Ruedy R, Sato M, Lo K (2010) Global surface temperature change. *Rev Geophys* 48:RG4004. <https://doi.org/10.1029/2010RG000345>
- Holland MM, Landrum L (2015) Factors affecting projected Arctic surface shortwave heating and albedo change in coupled climate models. *Philos Trans A R Soc* 373:20140162. <https://doi.org/10.1098/rsta.2014.0162>
- Holland M, Bitz C, Tremblay B (2006) Future abrupt reductions in the summer Arctic sea ice. *Geophys Res Lett*. <https://doi.org/10.1029/2006GL028024>
- Holland M, Baily DA, Vavrus S (2011) Inherent sea ice predictability in the rapidly changing Arctic environment of the Community Climate System Model, version 3. *Clim Dyn* 36:1239–1253. <https://doi.org/10.1007/s00382-010-0792-4>
- Holland M, Landrum L, Baily D, Vavrus S (2019) Changing seasonal predictability of arctic summer sea ice area in a warming climate. *J Clim* 32(16):4963–4979. <https://doi.org/10.1175/JCLI-D-19-0034.1>
- Hunke EC, Dukowicz JK (1997) An elastic-viscous-plastic model for sea ice dynamics. *J Phys Oceanogr* 27:1849–1867. [https://doi.org/10.1007/978-94-015-9735-7\\_24](https://doi.org/10.1007/978-94-015-9735-7_24)
- Jungclaus JH, Koenigk T (2010) Low frequency variability of the Arctic climate: the role of oceanic and atmospheric heat transport variations. *Clim Dyn* 34:265–279. <https://doi.org/10.1007/s00382-009-0569-9>
- Juszk I, Garcia M, Etchegorry J, Schaepman ME, Maximov TC, Strub G (2017) Drivers of shortwave radiation fluxes in Arctic tundra across scales. *Remote Sens Environ* 193:86–102. <https://doi.org/10.1016/j.rse.2017.02.017>
- Kapsch M, Graverson RG, Tjernstrom M, Bintania R (2016) The effect of downwelling longwave and shortwave radiation on Arctic summer sea ice. *J Clim* 29:1143–1159. <https://doi.org/10.1175/JCLI-D-15-0238.1>
- Kim J, Kim K (2019) Relative role of horizontal and vertical processes in the physical mechanism of wintertime Arctic amplification. *Clim Dyn* 52:6097–6107. <https://doi.org/10.1007/s00382-018-4499-2>
- Kim J, Kug J, Hoon J, Zeng N, Hong J, Jeong J, Zhao Y, Chen X, Williams M, Ichii K, Strub G (2022) Arctic warming-induced cold damage to East Asian terrestrial ecosystems. *Commun Earth Environ*. <https://doi.org/10.1038/s43247-022-00343-7>
- Large WG, Yeager SG (2008) The global climatology of an interannually varying air–sea fluxdata set. *Clim Dyn* 33:341–364. <https://doi.org/10.1007/s00382-008-0441-3>
- Large WG, McWilliams JC, Doney SC (1994) Oceanic vertical mixing: a review and a model with a nonlocal boundary layer parameterization. *Rev Geophys* 32(4):363–403. <https://doi.org/10.1029/94RG01872>
- Li Z, Ding Q, Steele M, Schweiger A (2022) Recent upper Arctic Ocean warming expedited by summertime atmospheric processes. *Nat Commun* 13:362. <https://doi.org/10.1038/s41467-022-28047-8>
- Liang X, Losch M (2018) On the effects of increased vertical mixing on the Arctic Ocean and sea ice. *J Geophys Res Oceans* 123:9266–9282. <https://doi.org/10.1029/2018JC014303>
- Linden EC, Bintanja R, Hazeleger W (2017) Arctic decadal variability in a warming world. *J Geophys Res Atmos* 122:5677–5696. <https://doi.org/10.1002/2016JD026058>
- Linden E, Bars D, Bintanja R, Hazeleger W (2019) Oceanic heat transport into the Arctic under high and low CO<sub>2</sub> forcing. *Clim Dyn* 53:4763–4780. <https://doi.org/10.1007/s00382-019-04824-y>
- Liu W, Fedorov A, Sevellec F (2019) The mechanisms of the Atlantic meridional overturning circulation slowdown induced by Arctic sea ice decline. *J Clim* 32(4):977–996. <https://doi.org/10.1175/JCLI-D-18-0231.1>
- Massonnet F, Vancoppenolle M, Goosse H, Dacqier D, Fichefet T, Wrigglesworth E (2018) Arctic sea-ice change tied to its mean state through thermodynamic processes. *Nat Clim Change* 08:599–603. <https://doi.org/10.1038/s41558-018-0204-z>
- Ming Z, Rong S, Ming D, Ping L (2021) Modeling turbulent heat fluxes over Arctic sea ice using a maximum-entropy-production approach. *Adv Clim Change Res* 12:517–526. <https://doi.org/10.1016/j.accre.2021.07.003>
- Muilwijk M, Smedsrud LH, Llicak M, Drange H (2018) Atlantic water heat transport variability in the 20th century Arctic Ocean from a global ocean model and observations. *J Geophys Res Oceans* 123:8159–8179. <https://doi.org/10.1029/2018JC014327>
- Murray RJ (1996) Explicit generation of orthogonal grids for ocean models. *J Comput Phys* 126:251–273. <https://doi.org/10.1006/jcph.1996.0136>
- Ohmura A (2012) Present status and variations in the Arctic energy balance. *Polar Sci* 6(1):5–13. <https://doi.org/10.1016/j.polar.2012.03.003>
- Oldenburg D, Armour KC, Thompson L, Bitz CM (2018) Distinct mechanisms of ocean heat transport into the Arctic under internal variability and climate change. *Geophys Res Lett*. <https://doi.org/10.1029/2018GL078719>
- Overland J, Dunlea E, Box JE, Corell R, Forsius M, Kattsov V, Olsen MS, Pawlak J, Reiersen L, Wang M (2019) The urgency of Arctic change. *Polar Sci* 21:6–13. <https://doi.org/10.1016/j.polar.2018.11.008>
- Parkinson CL, Comiso JC (2013) On the 2012 record low Arctic sea ice cover: combined impact of preconditioning and an August storm. *Geophys Res Lett* 40:1356–1361. <https://doi.org/10.1002/grl.50349>
- Perovich D, Richter-Menge J, Jones K, Light B, Elder B, Polashenski C, Laroche D, Markus T, Lindsay R (2011) Arctic sea-ice melt

- in 2008 and the role of solar heating. *Ann Glaciol* 52:355–359. <https://doi.org/10.3189/172756411795931714>
- Pickart RS, Spall MA (2007) Impact of Labrador Sea convection on the North Atlantic meridional overturning circulation. *J Phys Oceanogr* 37:2207–2227. <https://doi.org/10.1175/JPO3178.1>
- Poljakov IV, Alkire MB, Bluhm BA, Brown KA, Carmack EC, Chierici M, Danielson SL, Ellingsen I, Ershova EA, Gardfeldt K, Ingvaldsen RB, Pnyushkov AV, Slagstad D, Wassmann P (2020) Borealization of the Arctic Ocean in response to anomalous advection from sub-Arctic seas. *Front Mar Sci* 7:491. <https://doi.org/10.3389/fmars.2020.00491>
- Praetorius S, Rugenstein M, Persad G, Caldeira K (2018) Global and Arctic climate sensitivity enhanced by changes in North Pacific heat flux. *Nat Commun* 9:3124. <https://doi.org/10.1038/s41467-018-05337-8>
- Previdi M, Smith KL, Polvani LM (2021) Arctic amplification of climate change: a review of underlying mechanisms. *Environ Res Lett* 16:093003. <https://doi.org/10.1088/1748-9326/ac1c29>
- Proshutinsky A, Bourke RH, McLaughlin FA (2002) The role of the Beaufort Gyre in Arctic climate variability: seasonal to decadal climate scales. *Geophys Res Lett* 29(23):2100. <https://doi.org/10.1029/2002GL015847>
- Przybylak R, Wyszynski P (2020) Air temperature changes in the Arctic in the period 1951–2015 in the light of observational and reanalysis data. *Theor Appl Climatol* 139:75–94. <https://doi.org/10.1007/s00704-019-02952-3>
- Ramudu E, Yang R, Meneveau D, Gnanadesikan A (2018) Large eddy simulation of heat entrainment under Arctic sea ice. *J Geophys Res Oceans* 123:287–304. <https://doi.org/10.1002/2017JC013267>
- Ricker R, Kauker F, Schweiger A, Hendricks S, Zhang J, Paul S (2021) Evidence for an increasing role of ocean heat in Arctic winter sea ice growth. *J Clim* 34(13):5215–5227. <https://doi.org/10.1175/JCLI-D-20-0848.1>
- Serreze MC, Holland MM, Stroeve J (2007) Perspectives on the Arctic's shrinking sea ice cover. *Science* 315:1533–1536. <https://doi.org/10.1126/science.1139426>
- Shankar D (1998) Low-frequency variability of sea level along the coast of India. PhD thesis, Goa University, India. <http://shodhganga.inflibnet.ac.in:8080/jspui/handle/10603/31897>
- Smedsrud LH, Muilwijk M, Brakstad A, Maddonna E, Lauvset SK, Spensberger C, Born A, Eldevik T, Drange H, Jeansson E, Li C, Oslen A, Skagseth O, Slater DA, Straneo F, Vage K, Arthun M (2021) Nordic seas heat loss, Atlantic inflow, and Arctic sea ice cover over the last century. *Rev Geophys* 60:e2020RG000725. <https://doi.org/10.1029/2020RG000725>
- Steele M, Zhang J, Ermold W (2010) Mechanisms of summertime upper Arctic Ocean warming and the effect on sea ice melt. *J Geophys Res Oceans* 115:C11004. <https://doi.org/10.1029/2009JC005849>
- Stroeve J, Notz D (2018) Changing state of Arctic sea ice across all seasons. *Environ Res Lett* 13:103001. <https://doi.org/10.1088/1748-9326/aade56>
- Stroeve J, Holland MM, Meier W, Scambos T, Serreze M (2007) Arctic sea ice decline: faster than forecast? *Geophys Res Lett* 34:L09501. <https://doi.org/10.1029/2007GL029703>
- Stroeve JC, Serreze MC, Holland MM, Kay JE, Malanik J, Barret AP (2012) The Arctic's rapidly shrinking sea ice cover: a research synthesis. *Clim Change* 110:1005–1027. <https://doi.org/10.1007/s10584-011-0101-1>
- Swart NC, Fyfe JC, Hawkins E, Kay JE, Jahn A (2015) Influence of internal variability on Arctic sea-ice trends. *Nat Clim Change* 5:86–89. <https://doi.org/10.1038/nclimate2483>
- Timmermans M, Marshall J (2018) Understanding Arctic Ocean circulation: a review of ocean dynamics in a changing climate. *J Geophys Res Oceans* 125:e2018JC014378. <https://doi.org/10.1029/2018JC014378>
- Timmermans M, Marshall J (2020) Understanding Arctic Ocean circulation: a review of ocean dynamics in a changing climate. *J Geophys Res Oceans* 125:e2018JC014378. <https://doi.org/10.1029/2018JC014378>
- Tsubouchi T, Våge K, Hansen B, Larsen K, Øterhus S, Johnson C, Jonsson S, Valdimarsson H (2021) Increased ocean heat transport into the Nordic Seas and Arctic Ocean over the period 1993–2016. *Nat Clim Change* 11:1–6. <https://doi.org/10.1038/s41558-020-00941-3>
- Vialard J, Delecluse P (1998) An OGCM study for the TOGA decade. Part I: role of salinity in the physics of the western Pacific fresh pool. *J Phys Oceanogr* 28:1071–1088. [https://doi.org/10.1175/1520-0485\(1998\)028<1071:AOSFTT>2.0.CO;2](https://doi.org/10.1175/1520-0485(1998)028<1071:AOSFTT>2.0.CO;2)
- Vijith V, Vinayachandran PN, Webber BGM, Matthews AJ, George JV, Kannaujia VK, Lotliker AA, Amol P (2020) Closing the sea surface mixed layer temperature budget from in situ observations alone: operation advection during BoBBLE. *Nat Sci Rep* 10:7062. <https://doi.org/10.1038/s41598-020-63320-0>
- Wang X, Key J (2003) Recent trends in arctic surface, cloud, and radiation properties from space. *Science* 299:1725–1728. <https://doi.org/10.1126/science.1078065>
- Wang X, Key J (2005) Arctic surface, cloud, and radiation properties based on the AVHRR polar Pathfinder dataset. Part II: recent trends. *J Clim* 18:2575–2593. <https://doi.org/10.1175/JCLI3439.1>
- Wang C, Graham RM, Wang K, Gerland S, Granskog MA (2019) Comparison of ERA5 and ERA-Interim near-surface air temperature, snowfall and precipitation over Arctic sea ice: effects on sea ice thermodynamics and evolution. *Cryosphere* 13:1661–1679. <https://doi.org/10.5194/tc-13-1661-2019>
- Wang Q, Wekerle C, Wang X, Danlov S, Koldunov N, Sein D, sldorenko D, Appen W, Jung T (2020) Intensification of the Atlantic water supply to the Arctic ocean through Fram Strait induced by Arctic sea ice decline. *Geophys Res Lett* 47:e2019GL086682. <https://doi.org/10.1029/2019GL086682>
- Winton M (2000) A reformulated three-layer sea ice model. *J Atmos Ocean Technol* 17:525–531. <https://doi.org/10.1175/1520-0426>
- Wunderling N, Willeit M, Donges JF, Winkelmann R (2020) Global warming due to loss of large ice masses and Arctic summer sea ice. *Nat Commun* 11:5177. <https://doi.org/10.1038/s41467-020-18934-3>
- Zhang L, Li T (2017) Physical processes responsible for the interannual variability of sea ice concentration in Arctic in boreal autumn since 1979. *J Meteorol Res* 31(3):468–475. <https://doi.org/10.1007/s13351-017-6105-7>
- Zhang Y, Song M, Dong C, Liu J (2021) Modeling turbulent heat fluxes over Arctic sea ice using a maximum-entropy-production approach. *Adv Clim Change Res* 12(4):517–526. <https://doi.org/10.1016/j.accre.2021.07.003>
- Zou H, Gao Y, Langehaug H, Yu L, Guo D (2021) Thermodynamic processes affecting the winter sea ice changes in the Bering Sea in the Norwegian Earth System Model. *Ocean Sci*. <https://doi.org/10.5194/os-2021-16>

**Publisher's Note** Springer Nature remains neutral with regard to jurisdictional claims in published maps and institutional affiliations.

Springer Nature or its licensor holds exclusive rights to this article under a publishing agreement with the author(s) or other rightsholder(s); author self-archiving of the accepted manuscript version of this article is solely governed by the terms of such publishing agreement and applicable law.